OPTIMAL WIND CORRECTED FLIGHT PATH PLANNING FOR AUTONOMOUS MICRO AIR VEHICLES

THESIS

Michael D. Zollars, 1st Lieutenant, USAF

AFIT/GAE/ENY/07-M28

DEPARTMENT OF THE AIR FORCE
AIR UNIVERSITY

AIR FORCE INSTITUTE OF TECHNOLOGY

Wright-Patterson Air Force Base, Ohio

APPROVED FOR PUBLIC RELEASE; DISTRIBUTION UNLIMITED

The views expressed in this thesis are those of the author and do not reflect the official policy or position of the United States Air Force, Department of Defense, or the U.S. Government.

AFIT/GAE/ENY/07-M28

OPTIMAL WIND CORRECTED FLIGHT PATH PLANNING FOR AUTONOMOUS MICRO AIR VEHICLES

THESIS

Presented to the Faculty

Department of Aeronautics and Astronautics

Graduate School of Engineering and Management

Air Force Institute of Technology

Air University

Air Education and Training Command

In Partial Fulfillment of the Requirements for the

Degree of Master of Science in Aeronautical Engineering

Michael D. Zollars, BSME

1st Lieutenant, USAF

March 2007

APPROVED FOR PUBLIC RELEASE; DISTRIBUTION UNLIMITED.

AFIT/GAE/ENY/07-M28

OPTIMAL WIND CORRECTED FLIGHT PATH PLANNING FOR AUTONOMOUS MICRO AIR VEHICLES

Michael D. Zollars, BSME
1st Lieutenant, USAF

Approved:

Maj. Paul A. Blue (Thesis Advisor)	16 Mar 07 date
Dr. David R. Jacques (Committee Member)	16 MAR 07 date
Dr. Richard G. Cobb (Committee Member)	16 MAR 07 date

Abstract

This research effort focuses on determining the optimal flight path required to put a micro air vehicle's (MAVs) fixed sensor on a target in the presence of a constant wind. Autonomous flight is quickly becoming the future of air power and over the past several years, the size and weight of autonomous vehicles has decreased dramatically. As these vehicles were implemented into the field, it was quickly discovered that their flight paths are severely altered by wind. However, since the size of the vehicle does not allow for a gimbaled camera, only a slight perturbation to the attitude of the vehicle will cause the sensor footprint to be displaced dramatically. Therefore, the goal of this research was to use dynamic optimization techniques to determine the optimal flight path to place a MAV's sensor footprint on a target when operating in wind for three different scenarios. The first scenario considered the minimum time path given an initial position and heading and a final position and heading. The second scenario minimized the error between the MAV's ground track and a straight line to the target in order to force a desired path on the vehicle. The final scenario utilized both a forward mounted sensor as well as a side mounted sensor to optimize the time the target is continually in view of the sensor footprint. Each of these scenarios has been captured in simulated plots that depict varying wind angles, wind speeds, and initial and final heading angles. These optimal flight paths provide a benchmark that will validate the quality of future closed-loop wind compensation control systems.

Acknowledgments

I would like to express my deepest gratitude to my thesis advisor Major Paul Blue for his continued guidance and support. His drive and enthusiasm for research is captivating, and he was able to continuously motivate me throughout this research. His insight and knowledge in the subject matter proved to be invaluable to my success.

I must also express my thanks to all those who have given their support to this research effort; to include my peers in the ANT Lab as well as the officers of the March 2007 class. All of which could be counted on to provide necessary insight into the research at hand, or provide a much needed distraction to lighten the atmosphere during stressful times.

Most importantly, I must acknowledge my family. You have been committed to the success of this thesis, and have given me unconditional support throughout its entirety. Thank you for being who are and providing me with the strength to accomplish my goals. Finally to God, without whom nothing is possible.

Michael D. Zollars

Table of Contents

Page

Abstract iv
Acknowledgements v
Table of Contents vi
List of Figures ix
List of Tables xi
1. Introduction 1
1.1 Motivation 1
1.2 Problem Statement 3
1.3 Research Objectives 3
1.4 Significance of Research 4
1.5 Related Research 5
1.5.1 Aircraft Path Planning 5
1.5.1.1 Waypoint Following 6
1.5.1.2 Sensor Pointing with Wind Noise 7
1.5.1.3 Dubin Methodology 8
1.6 Solution Approach 10
1.7 Thesis Preview 12
2. Background 13
2.1 Overview 13
2.2 Aircraft 13
2.2.1 Micro Air Vehicles 14
2.2.2 Equipment Mounts 15
2.3 Dubins Path Planning 17
2.4 Discrete Dynamic Optimization 19
2.5 Simulation 22
2.6 Chapter Summary 23
3. Development of Optimal Trajectories to Autonomous Survey Targets 24
3.1 Overview 24

Page

3.2 Assumptions 24
3.3 Wind Calculations 24
3.4 Parameter Scaling 25
3.5 Dubins Path Calculation 26
3.6 Dynamic Optimization 31
3.6.1 Discretization Process 33
3.6.2 Problem Setup 34
3.6.3 Necessary Conditions for Optimality 35
3.7 Flight Path Variations 37
3.7.1 Minimum Flight Time with Forward Sensor 37
3.7.2 Minimum Flight Time with Side Sensor 38
3.7.3 Flight Path through an Urban Canyon 39
3.7.4 Continuous Tracking for Dual Sensors 41
3.8 Chapter Summary 43
4. Test Results and Analysis 44
4.1 Overview 44
4.2 Minimum Flight Time with Forward Sensor Results 44
4.3 Minimum Time Flight with Side Sensor Results 57
4.3.1 Flight Path Estimation 57
4.3.2 Optimization Results 59
4.4 Minimum Time Analytical Solution 62
4.5 Urban Canyon Results 64
4.5.1 Flight Path Estimation 65
4.5.2 Optimization Results 66
4.6 Target Tracking Results 78
4.6.1 Flight Path Estimation 79
4.6.2 Optimization Results 80
4.7 Chapter Summary 92
5. Conclusions and Recommendations 93
5.1 Conclusions 93

Page

5.2 Recommendations 95

Appendix A: MATLAB Code Explanation 97

Bibliography 103

Vita 105

List of Figures

Page

Figure 1 - Top View of UAV with Adjustment Parameters Defines (Robinson) 8
Figure 2 - Dubins Path Example with 50% Winds (McGee) 10
Figure 3 - TACMAV in Flight (USAF) 14
Figure 4 - TACMAV Flexible Wings (Higgs, 2005) 15
Figure 5 - Side and Top View of Vehicle with Forward Mounted Sensor 16
Figure 6 - Rear and Top View of Vehicle with Side Mounted Sensor 17
Figure 7 - Four Long Range Admissible Dubins Path 18
Figure 8 - Two Short Range Admissible Dubins Paths 19
Figure 9 - Dubins Initial Turn 27
Figure 10 - Dubins Final Turn 28
Figure 11 - Dubins Flight Path without Wind 29
Figure 12 - Dubins Path with Incorporated Wind 30
Figure 13 - Dubins Flight Path with Forward Sensor 31
Figure 14 - MAV Flight Angle Characterization 41
Figure 15 - Dubins Flight Path for Min Time Solution 45
Figure 16 - Optimized Flight Path for Min Time Solution 46
Figure 17 - Surface Plots - Varying Wind Heading with the Min Time Scenario 47
Figure 18 - Min Time Wind Heading vs Flight Time; Varied Wind Heading 48
Figure 19 - Min Time Aircraft Heading vs Wind Heading; Varied Wind Heading 49
Figure 20 - Min Time Aircraft Heading vs Flight Time; Varied Wind Heading 50
Figure 21 - Surface Plots - Varying Final Heading with the Min Time Scenario 51
Figure 22 - Min Time Target View Angle vs Flight Time; Varied Target Angle 52
Figure 23 - Min Time Aircraft Heading vs Target View Angle; Varied Target Angle 53
Figure 24 - Min Time Vehicle Heading vs Flight Time; Varied Target Angle 53
Figure 25 - Surface Plots - Varying Wind Speed with the Min Time Scenario 54
Figure 26 - Min Time Wind Magnitude vs Flight Time; Varied Wind Speed 55
Figure 27 - Min Time Vehicle Heading vs Wind Magnitude; Varied Wind Speed 56
Figure 28 - Min Time Vehicle Heading vs Flight Time; Varied Wind Speed 56
Figure 29 - Iteration of Dubins Path for Side Sensor 58
Figure 30 - Minimum Time Path for Dubins Estimation with Side Sensor 59
Figure 31 - Minimum Time Flight for Forward and Side Sensors, $\chi = 0,\ \beta = 0.5$ 60
Figure 32 - Minimum Time Flight for Forward and Side Sensors, $\chi = 180,\ \beta = 0.5$ 60

Page

Figure 33 - Minimum Time Flight for Forward and Side Sensors, $\chi = 270,\ \beta = 0.5$ 61
Figure 34 – Simulation for Analytical Solution 64
Figure 35 - Dubins Path Estimation for Urban Canyon Flight Path 65
Figure 36 - Optimization Solution for Urban Canyon Scenario 67
Figure 37 - Surface Plots - Varying Wind Heading with the Urban Canyon Scenario 68
Figure 38 - Urban Canyon Wind Heading vs Flight Time; Varied Wind Heading 69
Figure 39 - Urban Canyon Aircraft Heading vs Wind Heading; Varied Wind Heading 70
Figure 40 - Urban Canyon Vehicle Heading vs Flight Time; Varied Wind Heading 71
Figure 41 - Surface Plots - Varying Target Angle with the Urban Canyon Scenario 72
Figure 42 - Urban Canyon Wind Heading vs Flight Time; Varied Target Angle 73
Figure 43 - Urban Canyon Aircraft Heading vs Wind Heading; Varied Target Angle 74
Figure 44 - Urban Canyon Vehicle Heading vs Flight Time; Varied Target Angle 75
Figure 45 - Surface Plots - Varying Wind Magnitude with the Urban Canyon Scenario 76
Figure 46 - Urban Canyon Wind Heading vs Flight Time; Varied Wind Magnitude 77
Figure 47 - Urban Canyon Aircraft Heading vs Wind Heading; Varied Wind Magnitude 77
Figure 48 - Urban Canyon Vehicle Heading vs Flight Time; Varied Wind Magnitude 78
Figure 49 - Dubins Path for Dual Camera Scenario 79
Figure 50 - Forward Sensor Dual Camera for Variable Winds 81
Figure 51 - Dual Sensor Transition for Variable Winds 81
Figure 52 - Complete Dual Sensor Flight Path for Variable Winds 82
Figure 53 - Surface Plots - Varying Wind Heading with the Dual Sensor Scenerio 84
Figure 54 - Dual Sensor Wind Heading vs Flight Time; Varied Wind Heading 85
Figure 55- Dual Sensor Vehicle Heading vs Wind Heading; Varied Wind Heading 86
Figure 56 - Dual Sensor Vehicle Heading vs Flight Time; Varied Wind Heading 87
Figure 57 - Sensor Footprint Sensor for Varied Wind Heading 88
Figure 58 - Surface Plots - Varying Wind Magnitude with the Dual Sensor Scenerio 89
Figure 59 - Dual Sensor Wind Magnitude vs Flight Time; Varied Wind Magnitude 90
Figure 60 - Dual Sensor Vehicle Heading vs Wind Magnitude; Varied Wind Magnitude 90
Figure 61 - Dual Sensor Vehicle Heading vs Flight Time; Varied Wind Magnitude 91
Figure 62 - Sensor Footprint Radius for Varied Wind Magnitude 92

List of Tables

Page

Table 1 - Example of System Parameters with Dimensions 26
Table 2 – Optimization Problem Variables 32
Table 3 - Initial Parameters for the Minimum Time Scenario 44
Table 4 - Parameters to Compare Forward and Side Sensor 59
Table 5 - Forward Sensor vs Side Sensor Flight Time Results 61
Table 6 - Comparison of Analytical and Numerical Solution 64
Table 7 - Initial Parameters for the Urban Canyon Scenario 66
Table 8 - Initial Parameters for Dual Sensor Scenario 80

OPTIMAL WIND CORRECTED FLIGHT PATH PLANNING FOR AUTONOMOUS MICRO AIR VEHICLES

1. Introduction

1.1 Motivation

Over the past century, the United States has relied on the advancements of technology to aid in the development and efficiency of our culture. The military leads the effort in the majority of this research and development. When you consider the development of flight, it began in the 19th century when dirigibles were used for bombing missions, reconnaissance, and communication during wartime efforts. Later developments by the Wright Brothers led to the first powered heavier then air flight in 1903. Over the last century we have been led to the multi-role Joint Strike Fighter that is being designed to meet the needs of the Air Force, Navy, Marine Corps, and our Allies. Throughout this time, Unmanned Aerial Vehicles (UAVs) have been in development, and in the past twenty years, a strong effort has been made to continue research that focuses on their production and implementation. UAVs are quickly becoming the future of the Air Force as well as the military as a whole, as they can be utilized in circumstances and environments for which manned aircraft are unable to perform.

UAVs present numerous advantages over manned aircraft. They can be built to almost any shape and size. They can be flown into enemy territory or hazardous environments without endangering human life. And they can be utilized around the globe, at speeds and altitudes that humans cannot endure. For these reasons, and many

more, it is imperative that we continue the research and development into unmanned vehicles.

Micro-Air Vehicles (MAVs) are a subset of UAVs. These are aircraft built significantly smaller then current state of the art UAVs, such as the Global Hawk or Predator, and typically are electrically powered. One of the great benefits of a MAV is that it can be packaged into small containers, carried into the field by our military troops, and utilized as needed for surveillance or target tracking. Although this is a great asset to have, it brings up several issues that must be addressed. Since the vehicle is built to a very small size and weight, it is only capable of carrying an equally small and lightweight sensor. These sensors are typically mounted off the nose or belly of the aircraft, and because of the size, they are not capable of rotation. Therefore it becomes difficult to survey a ground target during flight. Any adjustments the vehicle makes could possibly cause the footprint of the sensor to lose track of its point of interest. Wind effects play a big role in this problem due to the extreme light weight of the aircraft. Only a small amount of wind is needed to throw the vehicle off course, resulting in the sensor footprint losing track of the target. Once these issues are solved and implemented, it will result in a great resource for our military in the field. These small aircraft will give our troops the capability to see around buildings, over hills, or hundreds of feet across the battlefield. Most important, it provides much needed surveillance in hostile environments which ultimately result in the reduced risk to human life.

1.2 Problem Statement

The proposed research effort will focus on developing flight path optimization techniques to enhance the Intelligence, Surveillance, and Reconnaissance (ISR) capabilities of MAVs in a constant wind environment. When dealing with miniature, light weight vehicles, wind effects can greatly disturb the desired flight path of the UAV. Additionally, when the MAV is equipped with a fixed sensor, it is imperative that the vehicle's orientation is such that the sensor footprint is focused on the point of interest. Often times in a wind environment, the vehicle will crab into the wind in order to maintain a desired ground track. In this situation, the nose of the aircraft will no longer be pointed in the desired direction, which will result in the sensor footprint failing to capture the requested information. Therefore, this research will focus on determining optimal wind corrected flight paths for surveying ground targets. The modeled system will be demonstrated and verified through software simulation and will incorporate multiple scenarios.

1.3 Research Objectives

Use optimization theory to determine the flight path that provides the optimum ground tack for a MAV's sensor footprint which adequately surveys the target of interest in a constant wind environment. Demonstrate the theory for several scenarios and show the accuracy and robustness of each. The results should focus on the ground track of the vehicle's sensor footprint.

- Determine the minimum time flight path for the MAV to put the footprint of a forward mounted sensor on a target given the MAV's initial condition (position and heading) and the targets position and required "look angle". Additionally, compare this minimum time path to one in which a side sensor of the MAV is utilized.
- Consider the case where the aircraft's flight path is restricted in width, as if the vehicle is flying in an urban canyon and must maintain flight down a road between two buildings. Once past the buildings, the aircraft should be able to adjust its flight path such that it can view a target at any desired angle.
- Utilize both a forward mounted sensor as well as a side-mounted sensor to continuously view the target for any duration of time. The algorithm should account for the transition between sensors such that the target is never lost.

1.4 Significance of Research

The optimal flight paths developed in this thesis show the best possible flight trajectories of a MAV given the problem objectives. Additionally, it provides a tool to be used with future work.

- These optimal paths provide a measure of performance with which future closed-loop wind compensated control systems can be compared.
- Many times, these aircraft are flown open-loop by the military operator in the field. By studying the optimal flight paths developed in this research, the MAV operators can become more efficient in accurately flying these aircraft.

- These results demonstrate what can be achieved with a MAV operating in winds. Additionally, it shows under what wind conditions the MAV will not be able to achieve the desired result. Furthermore, the results give an indication of the sensor equipment needed for various scenarios. It compares the utility of the forward sensor verses the side sensor, and provides an indication of the required footprint radius when orbiting a target.

1.5 Related Research

1.5.1 Aircraft Path Planning

Since using MAVs is relatively new for surveillance, there has been very little research in overcoming the wind effects on the flight path of these vehicles. The majority of the research that has been conducted to date consists of UAVs that are either large enough that wind will not greatly effect their flight patterns (Vaughn, 2003), or the vehicles are equipped with a gimbaled camera, for which you can control the orientation of the sensor as well as the orientation of the vehicle (Rafi, 2006 and Rysdyk, 2006). The research conducted for this thesis will consider small lightweight MAVs that only have the capability of carrying lightweight fixed sensors. Since the sensor is fixed, it requires the flight of the aircraft to be controlled so that the target will be in view of the sensor's footprint. Only a few papers have been found that relate to these issues. These papers have determined wind algorithms to adjust the aircraft in flight by flying the MAV on a waypoint trajectory where each target is located at a waypoint (Robinson, 2006 and Osborne, 2005). However, little work has been done when utilizing a fixed sensor

mounted on the air vehicle for surveillance. Additionally, these methods do not address optimality and do not provide a measure of performance, as will be discussed herein.

1.5.1.1 Waypoint Following

In autonomous flight, it is very common to fly the vehicle along a path defined by a series of waypoints. However, when considering unmanned aircraft, wind will have a very significant nonlinear effect that will greatly disturb the orientation and ground track of the vehicle.

Therefore it becomes very difficult to accurately follow pre-determined waypoints in the presence of wind. However, waypoint guidance could be used to fly the flight paths developed in this thesis. Determining the optimal flight path is only half the problem. Once that flight path has been determined for a certain wind field, flight along that path can be achieved by flying the path defined by several waypoints.

In research conducted at the University of Washington, Osborne and Rysdyk have studied methods to not only allow an unmanned vehicle to follow waypoints, but to do so with little or no overshoot in the presence of wind. The problem they encountered was that "in un-anticipatory waypoint flying, once a waypoint has been achieved, the aircraft begins a turn to the next waypoint. This results in an overshoot of the desired flight path, which can be substantial" (Osborne, 2005 and Rysdyk, 2006). In an attempt to eliminate this overshoot, they determined a 'look ahead' distance which defines the distance at which the aircraft should begin to turn in order to accurately adjust to the next waypoint. This distance is determined by a pre-calculated look-up table that will account for course change, wind direction, wind speed and commanded airspeed (Osborne, 2005 and

Rysdyk, 2006). This method has shown a drastic reduction in flight path overshoot of pre-determined waypoints, which ultimately will result in the flight of a more optimum path.

In research conducted at the Air Force Institute of technology, Ensign Brent Robinson applied an updating "Rabbit" waypoint placement approach to account for non-constant winds. His research showed that by knowing the horizontal distance between the aircraft's current position and a point of interest, a waypoint could be determined based on the current wind conditions. The aircraft would then attempt to fly to this continuously updating waypoint, however would never reach it. Instead, the aircraft would end up at the original point of interest. Therefore this approach consists of a vehicle attempting to chase a rabbit, but never actually catching it (Robinson, 2006). Furthermore, it provides an additional method of flying the optimal flight paths in the presence of wind developed in this thesis.

1.5.1.2 Sensor Pointing with Wind Noise

Ensign Brent Robinson continued his research to consider the issue of placing the footprint of a small fixed sensor attached to a MAV on a target of interest in the presence of wind. He acknowledged the problem that as MAVs attempt to fly in a wind environment, the vehicle will be forced to "crab" into the wind in order to remain on its current flight path. However, due to this crab angle, the vehicle no longer will have its sensor's footprint pointed at the target of interest. In order to solve for this offset, he defines two distances to adjust for the crab angle. Figure 1 shows these two distances as Adjust 1 and Adjust 2.

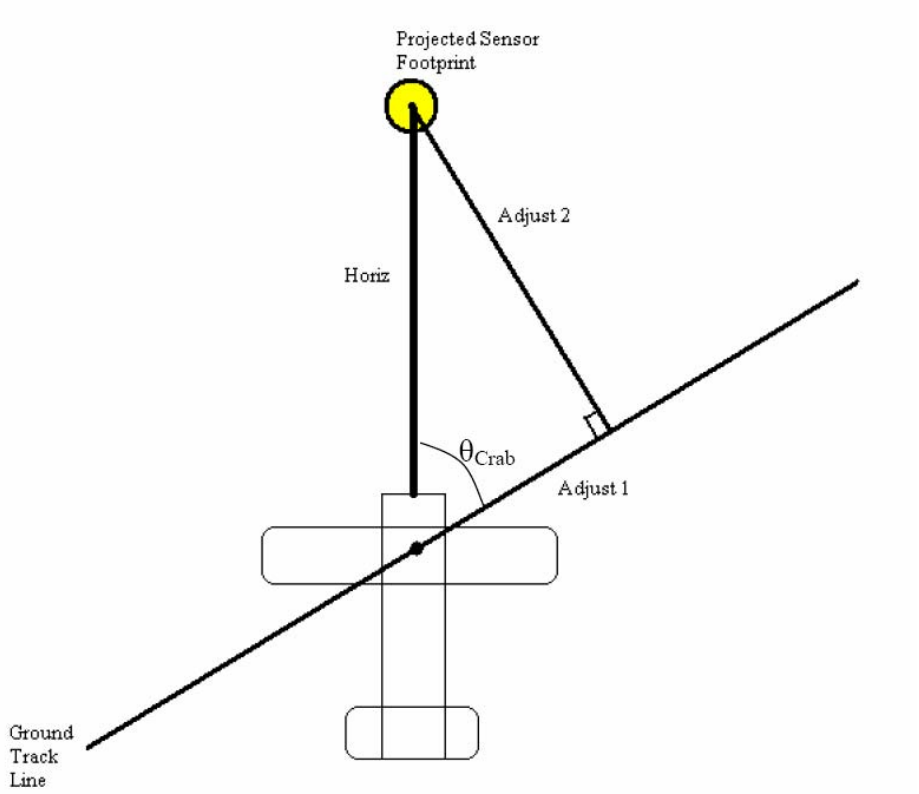

Figure 1 - Top View of UAV with Adjustment Parameters Defines (Robinson)

By knowing these two distances, they can then be added or subtracted to the target position as necessary to provide for an offset flight path that would allow for the sensor to survey the target (Robinson, 2006).

1.5.1.3 Dubin Methodology

L. E. Dubin developed a method for determining the shortest distance between two points given an initial position and heading to a final position and heading. He considered an object, defined as a point mass, that follows a continuous differentiable path, with the assumption that the turn radius of the object is fixed. He showed that the shortest path taken will consist of not more than three pieces, each for which is either a

straight line segment or an arc of a constant radius (Dubins, 1957). Many others have adopted his philosophy and used it in their own work. McGee, Spy, and Hedrick, out of the University of California Berkeley, determined optimal path planning in the presence of wind using Dubins methods (McGee, 2005). Their work consisted of first finding the optimal set of curves and straight lines to reach a target. Once that was accomplished, they gave the target a virtual velocity equal and opposite to that of the wind. Using an iterative approach, they solved for the Dubins Path at each time step, until the time of the aircraft's flight equaled the time of the virtual target's flight. At the final step, the air path of the vehicle would be exactly on the moving virtual target; however, the ground path of the vehicle would be exactly on the original target point. An example of this method can be seen from McGee, Spy, and Hedrick's work in Figure 2 below which shows a left curve, straight line, right curve path in the presence of fifty-percent winds. The virtual target traveled to a final position of (1.5,1) while the actual target is at position (5,1).

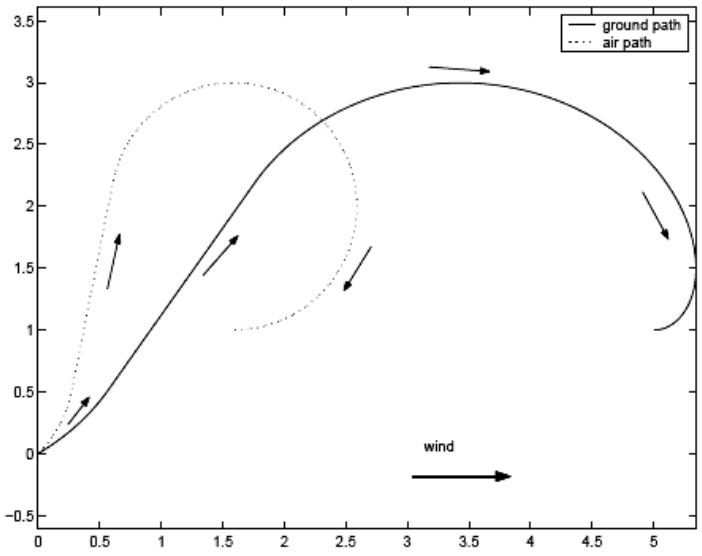

Figure 2 - Dubins Path Example with 50% Winds (McGee)

1.6 Solution Approach

Utilizing the previous work performed and researched in the control and optimization of aircraft trajectories, this thesis will develop a method for optimal flight path planning of MAVs. Initially, the parameters of the problem will be defined and those parameters will be non-dimensionalized such that the simulation can be run for any desired scenario. This gives the ability to trace a simulation to either metric or standard units. The next step is to develop a process for determining a good estimation of the flight path. This is a necessity when working with optimization software such as the optimization toolbox in Matlab. The estimated path will be produced using the theories of L.E. Dubins along with the path planning techniques of McGee, Spy, and Hedrick.

With an initial guess built for the flight path, an optimization problem can be set up utilizing the initial guess as a starting point for the optimal control problem. The first

problem that will be considered is the minimum time flight from a starting position and heading to a final position and heading in the presence of a constant wind. Using the function *fmincon*, within the Optimization Toolbox of Matlab, an optimal solution will be found. This minimum time case will be conducted for both a forward mounted sensor as well as a side mounted sensor. Comparing these flight times will lend to a better understanding of the utility of the sensors, and when it may be beneficial to use one sensor over the other. In addition to the numerical solution, the problem will be evaluated analytically in an attempt to determine the validity of the optimal results and ultimately solve for a closed-form solution to the problem.

The second scenario that will be evaluated will consider flight through an urban canyon. This will consist of flying the aircraft down a straight path, as if flying between two buildings. Again, the aircraft should be able to start at any position and heading, and view the target with a forward mounted sensor at any desired angle. To solve this problem, the flight path objective will need to be altered from the minimum time scenario described above. The new cost function will force the aircraft to fly a straight line ground path to the target. This additional path constraint will optimize the point at which the vehicle leaves the straight line path and places the footprint of the forward mounted sensor on the target at the commanded angle.

The final scenario will utilize both a forward mounted sensor as well as a side mounted sensor to first find the target in a minimum time fashion, and then track the target for any desired amount of time. This scenario will be comprised of three paths. The first path considered minimum time flight to get the forward mounted sensor on the target as quickly as possible, regardless of the viewing angle. The second path is a

minimum time path that transitions the forward sensor on the target to the side sensor on the target. Now, with the side sensor on the target, the final path consists of an orbit around the target that maximizes the time the sensor footprint is placed on the target. All three paths will account for a constant wind disturbance.

1.7 Thesis Preview

Chapter 2 will detail the equipment used and mathematical processes required for the research. Chapter 3 will look at the approach to solving each objective. Chapter 4 will discuss the results of each optimization. Chapter 5 will provide a summary, conclusion, and recommendations for future work.

2. Background

2.1 Overview

Chapter 2 provides background information on the aircraft that will be used for this research as well as the methodology behind dynamic optimization and path planning. This chapter builds a foundation for which the remainder of the paper can be understood. Initially the aircraft for which this research is built around is identified. This is followed by a discussion of optimal path planning using methods developed by L.E. Dubins as well as dynamic optimization. Finally the chapter concludes with a description of the optimization setup and procedures in the Matlab optimization software.

2.2 Aircraft

Timely and accurate surveillance is crucial for today's military. Whether it is the need for target surveillance, battle damage assessment following a strike, or a scout to view what lies ahead, an expandable pair of eyes to monitor the battle zone is an incredible benefit to our military. In the past, the military has utilized larger UAVs such as the Predator or the Global Hawk. However, these aircraft are quite large and require a great deal of coordination to be flown. They cannot be used effectively at the small unit level in the field. The MAV presents a new class of vehicles that have been developed to provide further information at the tactical level. These aircraft have been designed to be hand carried into the field, utilized at will by a single military member, and retrieved undamaged. They have the capability of providing close proximity information that could be crucial to the mission's success.

2.2.1 Micro Air Vehicles

The Munitions Directorate of the Air Force Research Lab has developed a light-weight aircraft for military surveillance in the battlefield. The TACtical MAV (TACMAV), seen below in Figure 3, was first flown in 2003 and has been issued to the warfighter for field testing (Roadmap, 2005). This hand-launched vehicle is battery operated and navigates using a GPS/INS system. The vehicle utilizes two sensors for surveillance. One is mounted at a 45 degree angle directed out the nose and the other is mounted at a 30 degree angle directed out the wing. The operator of the TACMAV uses a ruggadized notebook to control the vehicle in flight as well as view target information. Continuous improvements and research are addressing the vehicles autopilot, sensors, and control systems.

Figure 3 - TACMAV in Flight (USAF)

The current configuration of the TACMAV is equipped with flexible carbon fiber wings, shown in Figure 4, which have the capability to curl under the fuselage for easy

storage in a nine inch diameter tube. These flexible wings reduce the span-wise storage requirements by over sixty percent (Higgs, 2005).

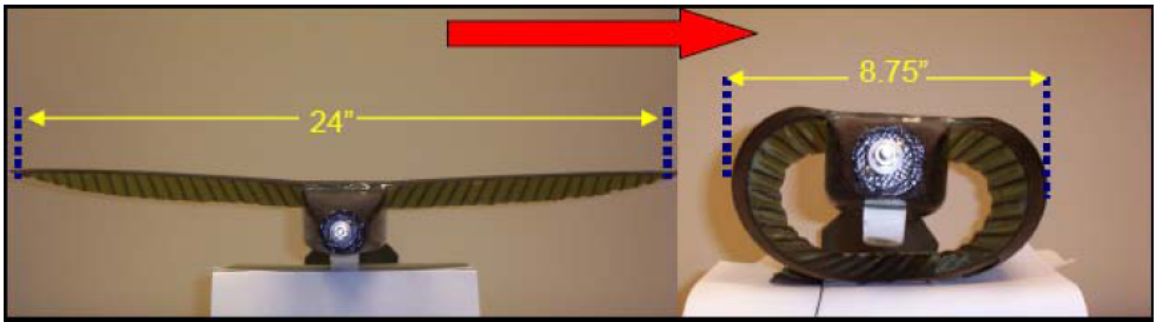

Figure 4 - TACMAV Flexible Wings (Higgs, 2005)

2.2.2 Equipment Mounts

The lightweight TACMAV is equipped with sensors capable of viewing ground targets both directly in front, as well as out the side of the aircraft. However, this aircraft is very susceptible to wind disturbance which significantly decreases the ability to accurately point its sensor directly at the target at the desired approach angle. For initial scenarios, only the sensor mounted off the nose of the aircraft will be considered. Figure 5 depicts the sensor configuration for steady level flight with a constant flight altitude. Equation 1 and 2 describes the position of the sensor footprint, (x_s, y_s), given the current position, (x_p, y_p), and heading, θ, of the aircraft measured from East. Equation 3 describes the vertical angle the sensor is mounted off the aircraft which results in the forward distance the footprint appears in front of the aircraft. For this research $\mu = 45^o$, which with a constant altitude, results in a constant d_N.

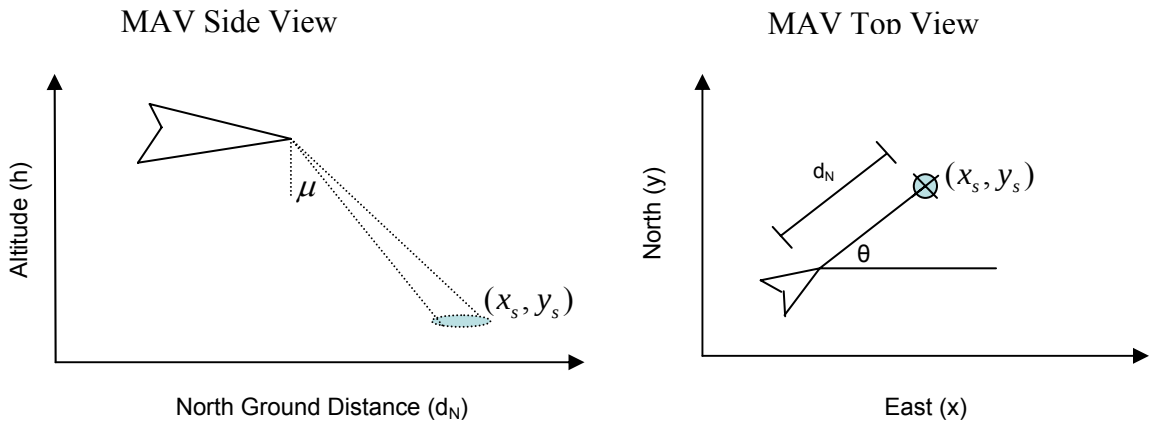

Figure 5 - Side and Top View of Vehicle with Forward Mounted Sensor

$$x_s = x_p + d_N * \cos\theta(i) \quad \textbf{(1)}$$

$$y_s = y_p + d_N * \sin\theta(i) \quad \textbf{(2)}$$

$$\tan\mu = d_N / h \ \ \therefore \ d_N = h * \tan(\mu) \quad \textbf{(3)}$$

Additional simulations will be conducted in which the side sensor of the TACMAV will be employed. Below, Figure 6 depicts the side sensor configurations for steady level flight at a constant altitude. Equation 4 describes the angle the side sensor is mounted off the aircraft which results in the perpendicular distance the footprint appears to the side of the aircraft. Equation 5 relates the vehicle's heading, θ, to the heading angle of the sensor, ψ. Finally, the position of the sensor footprint, $(\overline{x}_s, \overline{y}_s)$, is described in Equations 6 and 7 by using the aircraft's position, $(x_{p,} y_p)$, as well as the sensor angle.

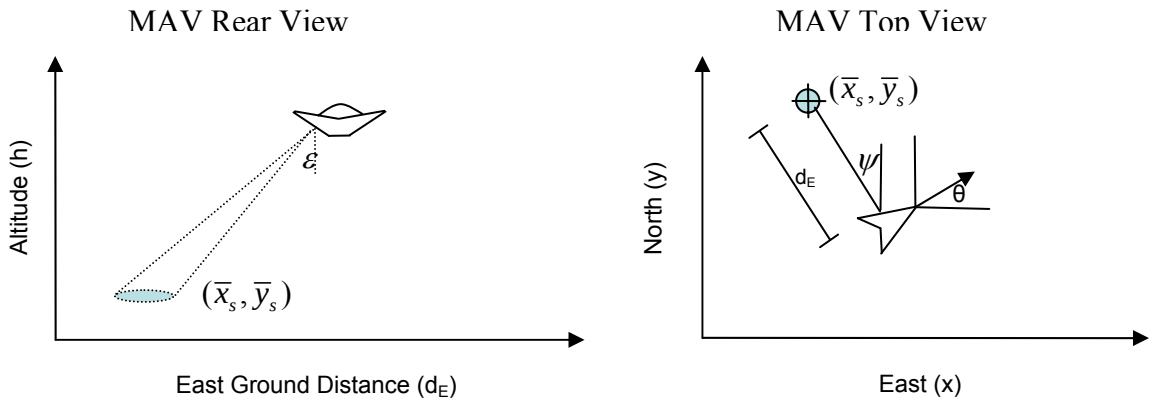

Figure 6 - Rear and Top View of Vehicle with Side Mounted Sensor

$$\tan\varepsilon = d_E / h \quad \therefore \quad d_E = h * \tan(\varepsilon) \tag{4}$$

$$\psi = \theta + \pi/2 \tag{5}$$

$$\overline{x}_s = x_p + d_E \cos\psi(i) \tag{6}$$

$$\overline{y}_s = y_p + d_E \sin\psi(i) \tag{7}$$

2.3 Dubins Path Planning

L.E. Dubins determined the minimum length for curves with a constant average curvature and a prescribed initial and terminal position and heading. His theory is based off of a particle pursing a continuous, differentiable path from an initial point to a final point at a constant speed. His objective was to determine the path of minimum length. Dubins claims that it is natural to require the path to have curvature in its entirety and that the radius of that curvature would have to be equal to or greater than a fixed number *R*. He then describes an R-geodesic as the path of minimum length that must exist between two points given an initial and final position and heading. Therefore, his

research is described in that “Theorem 1, which implies that for $n = 2$; an R-geodesic is necessarily a continuously differentiable curve which consists of not more than three pieces, each for which is either a straight line segment or an arc of a circle of radius R. Furthermore, the corollary to Theorem 1 implies that three is the least integer for which this is true” (Dubins, 1957).

Given the assumption that the initial and final position are more than $2R$ distance apart, and you have a specified initial and final heading, then the minimum length path will be one of four path lengths. The four minimum path options are limited to an initial curve of radius R, followed by a straight line, and completed with a curve of radius R. Dubins describes these four types as Right-Straight-Right (RSR), Left-Straight-Left (LSL), Right-Straight-Left (RSL), and Left-Straight-Right (LSR) (McGee, 2005). All four of these options are shown below in Figure 7.

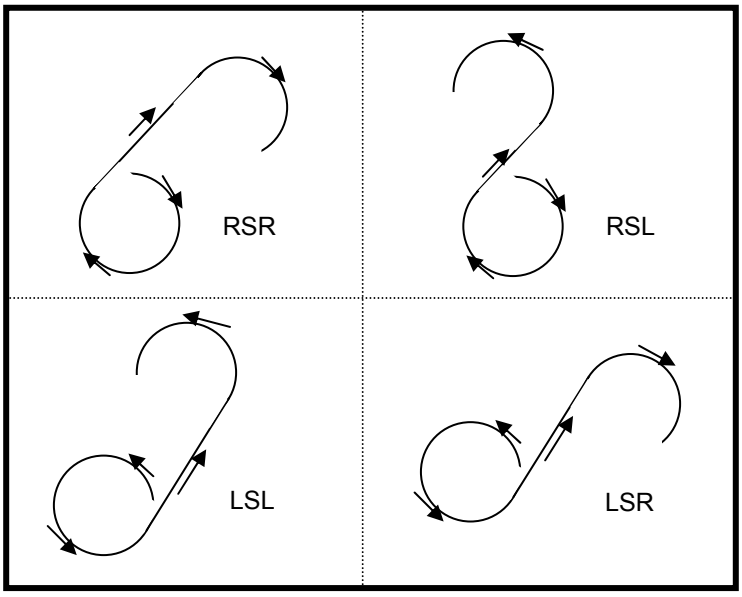

Figure 7 - Four Long Range Admissible Dubins Path

Considering the case where the initial and final positions are in close proximity, that is the final position is within 2*R*, the shortest path will be a series of three curves of radius *R*. These paths are described as Right-Left-Right outer (RLR_{outer}) and Left-Right-Left outer (LRL_{outer}) (McGee, 2005). An illustration of the two paths is given below in Figure 8.

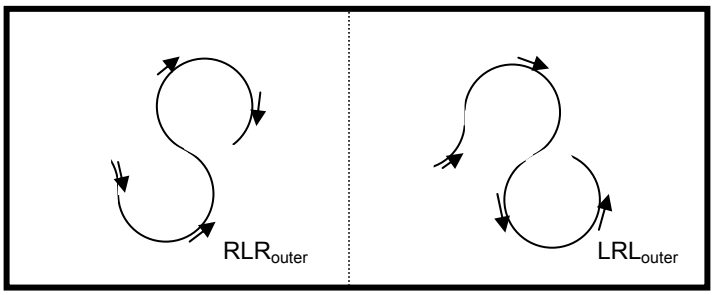

Figure 8 - Two Short Range Admissible Dubins Paths

In all, this presents six solutions that will get the aircraft from its initial conditions to its final conditions. Furthermore, one of these six paths will be the optimal Dubins Path.

2.4 Discrete Dynamic Optimization

Dynamic Optimization is a process that uses calculus of variations or dynamic programming to solve many different classes of problems. The three primary problems are given a fixed final time and free final state, a fixed final time and fixed final state, and a free final time and fixed final state. For the purpose of this research, only the free final time, fixed final state case will be discussed.

Dynamic Optimization is the process of determining control and state histories for a dynamic system over a finite time period to minimize a performance index (Bryson, 1999). It is often used to solve for the optimum control given the cost function pertaining

to aircraft, spacecraft, or robotics. Additionally, it is quickly becoming a common practice to solve optimization problems using discretized equations of motion due to its compatibility with computer simulation and flexibility with different problem scenarios (Larson, 2005). The process for discretization is further discussed in Chapter 3.

A discrete dynamic optimization system is described using an *n*-dimension state vector $x(i)$ at step i ,for $i = 1, 2, ..., N$, using the Bolza formulation (Bryson, 1999). The states, of the form seen in Equation 8 below, consist of discretized equations of motion that describe the optimization problem.

$$x(i+1) = f(x(i), u(i), \triangle t) \tag{8}$$

With the initial boundary conditions given by,

$$x(0) = x_0 \tag{9}$$

The control of the system, $u(i)$, is an *m*-dimension vector that determines the transition of the system to the state (Bryson, 1999). The optimization is then performed by finding a sequence of control to minimize the objective function J , described below in Equation 10, subject to terminal constraints given in Equation 11, the initial conditions given in Equation 9, and the state equations given in Equation 8 (Bryson, 1999).

$$J = \phi(x(N), \triangle t) + \sum_{i=1}^{N} L(x(i), u(i), \triangle t) \tag{10}$$

$$subject\ to\ \ \psi[x(N)] = 0 \tag{11}$$

The objective function, which includes a terminal cost $\phi(x(N), \Delta t)$ and a path cost $L(x(i), u(i), \triangle t)$, is a function of the states, the control, and the final time, while the

terminal constraints are functions of only the final states. Equations 9 through 11 define a dynamic optimization problem that can be transformed into a parameter optimization problem with equality constraints that can be solved by providing an initial guess of the control vector $u(i)$, calculating the values of the states, and then determining the value of the cost function J.

To obtain an analytic solution, define a discrete Hamiltonian, which is formed by adjoining the state equations to the path cost to obtain,

$$H(x(i),u(i),\triangle t) = L(x(i),u(i),\triangle t) + \lambda^T(i+1) f(x(i),u(i),\triangle t) \quad (12)$$

The co-states of the system are then found by taking the gradient of the Hamiltonian (12) with respect to each state *x*.

$$\lambda^T(i) = H_x(i) = L_x(i) + \lambda^T(i+1) f_x(i) \quad \textbf{(13)}$$

The final co-states, described in Equation 14, are determined by taking the gradient of the terminal cost with respect to each state *x*. By knowing the final co-states, Equation 13 can be sequenced backwards for a solution at each increment.

$$\lambda\ (N) = \phi_x \quad \textbf{(14)}$$

Next, the optimality criterion, H_u, is found by taking the gradient of the Hamiltonian with respect to the control $u(i)$.

$$H_u(x(i),u(i),\triangle t) = L_u(x(i),u(i),\triangle t) + \lambda^T(i+1) f_u(x(i),u(i),\triangle t) = 0 \quad \textbf{(15)}$$

When considering free final time problems, an additional equation is needed to solve for the $\triangle t$ variable. This equation is know as the transversality criterion and is expressed

below in Equation 16. It is found by taking the gradient with respect to Δt of both the augmented terminal cost and the summation of the Hamiltonian at each time step. The augmented terminal cost is designated as $\Phi(x(N),\Delta t)$, which is equal to the terminal cost added to the final co-states adjoined with Lagrange multipliers.

$$\Phi_{\Delta t}(x(N),\Delta t)+\sum_{i=0}^{N-1}[L_{\Delta t}(x(i),u(i),\Delta t)+\lambda^{T}(i+1)\,f_{\Delta t}(x(i),u(i),\Delta t)]=0 \qquad \textbf{(16)}$$

Equations 15 and 16 are known as the necessary conditions for optimality for a free final time solution.

To solve for a control vector sequence $u(i)$ that minimizes the objective function (10), the discrete Euler Lagrange equations (8) and (13) must be solved along with the necessary conditions of equations (15) and (16). The result will be a control vector that will minimize the objective function based on the initial conditions to the states and the values of the final co-states (Bryson, 1999).

2.5 Simulation

All simulations for this research were conducted in Matlab Version 7 (R14). The discrete dynamic optimization results were calculated using the Optimization Toolbox's *fmincon* function. The *fmincon* function, called with the appropriate arguments and options, will return an optimum solution to a function of several variables. Two M-files are required by the function. The first is of the objective function which describes the cost of the system. The second includes the constraints placed on the final states. For the

purpose of this research, finite differences were used in the numerical solution to calculate gradients.

2.6 Chapter Summary

This chapter reviewed all of the equipment, mathematical techniques, and software used in the overall research for this subject matter. The TACMAV was described as the vehicle of interest and its capabilities and sensor mounts were discussed. Discrete dynamic optimization was portrayed as the optimal solution technique and the Dubins path method was laid out as providing an initial guess to the optimal solution. Finally, Matlab and the Optimization Toolbox were selected to solve the discrete optimization problem posed.

3. Development of Optimal Trajectories to Autonomous Survey Targets

3.1 Overview

This chapter lays out the fundamental equations and processes for optimal flight path planning under constant wind disturbance. With an overhead view of the aircraft's flight path, the equations of motion as well as the vehicle's relationship to the sensor footprint can be determined using basic trigonometric functions. Dynamic optimization principles are used in an attempt to verify the numerical solution to the optimum path.

3.2 Assumptions

The following assumptions were made during the course of this research:

1. The aircraft is modeled as a point mass
2. The sensor footprint is modeled as a point source
3. The front camera is fixed and mounted with $\mu = 45$ degrees, therefore $h = d_N$
4. The side camera is fixed and mounted with $\varepsilon = 30$ degrees, therefore $h \neq d_E$
5. The aircraft will fly at a constant airspeed
6. The wind will be constant in both direction and magnitude for a given flight

3.3 Wind Calculations

The wind will be constant in magnitude and heading for both the Dubins path optimization as well as the dynamic optimization. As seen in Equation 17, beta will

describe the ratio of the magnitude of the wind to the magnitude of the aircraft's airspeed. χ defines the direction of the wind from east, as shown in Equation 18.

$$\beta = \frac{Wind_{mag}}{V_{Aircraft}} \tag{17}$$

$$\chi = Wind_{Direction} \tag{18}$$

With the winds direction and magnitude defined, the wind in the north direction, W_x, and the wind in the east direction, W_y, can be calculated.

3.4 Parameter Scaling

In the given problem, there are three key parameters; velocity, turn radius, and altitude. Of these parameters there are two dimensions associated; time and distance. For parameter scaling, one of the three parameters must be expressed in terms of another. For this research, the velocity and the turn radius where scaled to one and the altitude will be expressed in the number of turn radiuses. For the generic portion of the simulations, the parameters will be set as follows:

$$Velocity = V = 1 \tag{19}$$

$$Turn\ Radius = r = 1 \tag{20}$$

$$Altitude = d = 5 * r \tag{21}$$

The time unit will be defined as the time required to fly one radius, and is given by the distance, r, divided by the velocity, V, which in this case will be one.

To incorporate dimensions into the problem, a value must be chosen for the velocity and either the altitude or the turn radius as outlined in Equations 19 through 21.

With these two values chosen, the values and dimensions can be calculated for the turn rate and the time unit using Equations 22 and 23 below.

$$\omega = turn\ rate = \frac{V\ [\frac{length}{time}]}{R\ [length]} \tag{22}$$

$$t = time\ unit = \frac{R\ [length]}{V\ [\frac{length}{time}]} \tag{23}$$

The total time can be calculated by multiplying the time unit by the total number of time steps, N . An example of the dimensionalization process is described below in Table 1.

Table 1 - Example of System Parameters with Dimensions

Parameter	Non-Dimensionalized	Dimensionalized
V - Velocity	1 [length/time]	choose V = 20 ft/sec
R - Turn Radius	1 [length]	choose R = 40 ft
d - Altitude	5*R [length]	d = 200 ft
ω - turn rate	V/R [radians/time]	ω = 0.5 rad/sec
t - time unit	R/V [time]	t = 2 sec

This example illustrates the typical flight parameters of a MAV, and were considered as practical values for the purpose of this research. However, these parameters could be scaled to any dimension desired for future work.

3.5 Dubins Path Calculation

One of the major issues of dynamic optimization is that it requires a realistic guess of the correct flight path and time of flight to converge to an optimum answer. Therefore a method was developed to give the optimization routine a good estimate of the vehicle's flight path. This estimate was developed using a Dubins path routine. The Dubins path

routine is based on the concept that the shortest path to get from point A to point B is a straight line. When you consider an initial and final heading angle, the shortest path becomes a set of two curves of minimum radius and a straight line. This procedure was developed as follows:

- At the starting point of the aircraft, the vehicle can do one of three things, minimum turn radius left, minimum turn radius right, or fly straight. Therefore, as shown in Figure 9, two circles of minimum radius were constructed as optional flight paths for the initial curve. To demonstrate, the initial conditions were given as a starting point of $x_p = 0$, $y_p = 0$, and $\theta_o = 90^o$.

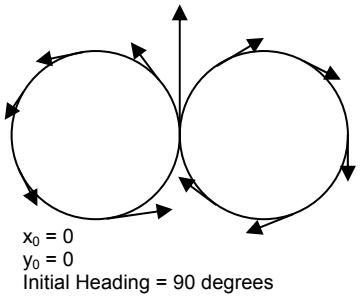

Figure 9 - Dubins Initial Turn

- The same concept applies when the vehicle arrives at the target. It can fly straight into the target, make a left turn to arrive at the target, or make a right turn to arrive at the target. Again, two minimum turn radius circles were constructed as optional flight paths for the final curve as shown in Figure 10. The final conditions were given as $x_p = 6$, $y_p = 8$, and $\theta_N = 180^o$.

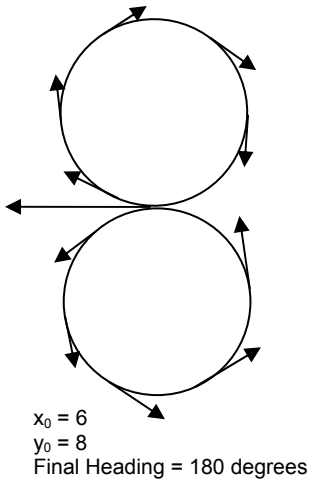

Figure 10 - Dubins Final Turn

- To complete the path, four iterations were conducted, one from each starting circle to each final circle. For each of the four iterations, the algorithm searched until the tangent vector of the initial circle equaled the tangent vector of the final circle. Once those vectors were determined, a line was drawn to connect the circles at the respective points and the final path was drawn. In total, four tangent lines were drawn, one from each initial circle to each final circle as seen below in Figure 11. One of those four paths is the shortest distance from the initial position and heading to the final position and heading.

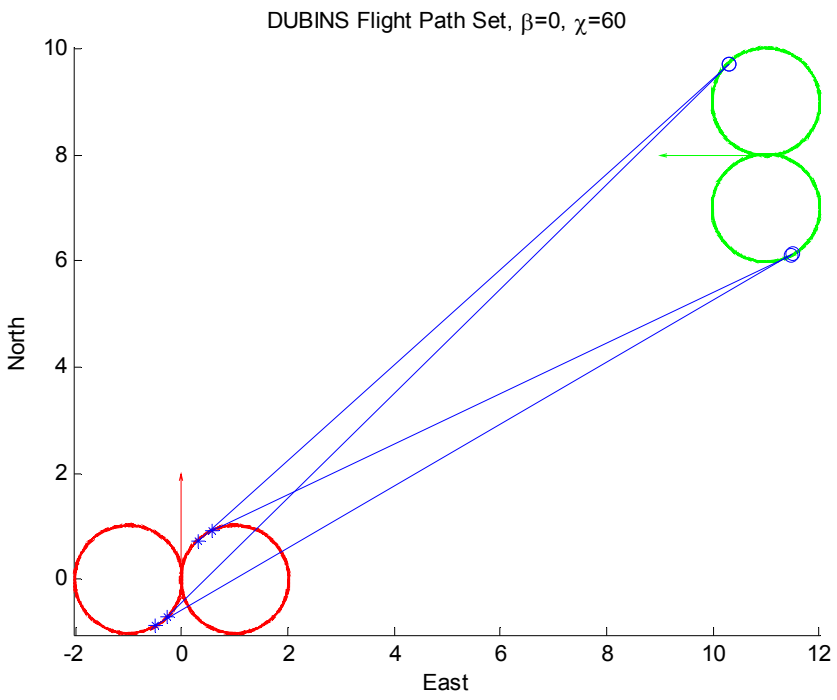

Figure 11 - Dubins Flight Path without Wind

Now that a process for the shortest path has been determined, next the wind must be incorporated. For the Dubins path model, a virtual moving target will account for the wind. The virtual target will be given a velocity and heading equal and opposite to that of the wind (McGee, 2005). Therefore as the aircraft attempts to put its sensor on the virtual target, in actuality, since the wind has altered the vehicle's flight path, the sensor will be directly over the actual target. In other words, the air path of the vehicle's sensor will approach the virtual target; however, the ground path of the vehicle's sensor will approach the actual target.

The final obstacle was to determine how far the virtual target should travel before it would be intercepted by the aircraft's sensor footprint. This was accomplished in an iterative approach with the time of flight of both the aircraft and the target. Once the

simulation is started, the Dubins path is calculated from the initial point and heading to the virtual target at each time step. Therefore, as the virtual target continues to move equal and opposite to the wind, a new Dubins path is calculated. Once the time of flight of the aircraft is equal to the time of flight of the virtual target, the final Dubins path is calculated. Figure 12 below shows the same simulation as in Figure 11, however now the aircraft must overcome a constant wind with $\beta = 0.2$ and $\chi = 60^o$.

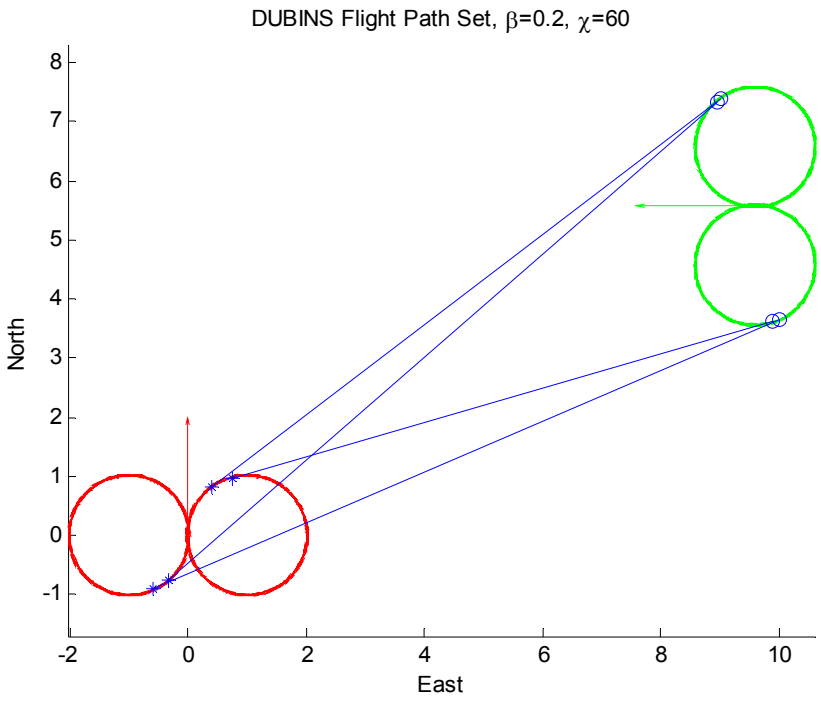

Figure 12 - Dubins Path with Incorporated Wind

With the wind incorporated, the shortest flight path is calculated and the sensor footprint is added into the algorithm as a fixed offset from the aircraft. Figure 13 displays the vehicle's air path as well as the vehicle's ground path. In addition to the ground path, the asterisk depicts the position of the sensor footprint at each time step. The square indicates the final target position. The virtual target path depicts the final

position of the aircraft without regard to the offset distance required by the sensor footprint.

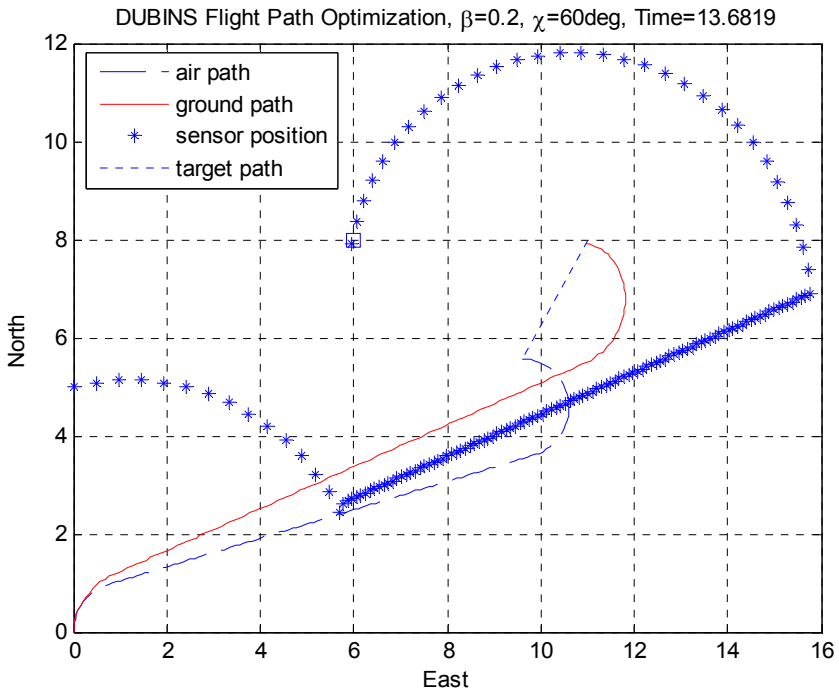

Figure 13 - Dubins Flight Path with Forward Sensor

Now that the Dubins path model produces a realistic flight path, these results can be input as the initial flight path estimate for the dynamic optimization problem. This guess is best utilized for the minimum time cost function. Any changes to the cost function, that may include a path cost, may need a better guess for *fmincon* to accurately solve for the optimal flight path.

3.6 Dynamic Optimization

Dynamic optimization was used in this research to solve three different problem scenarios; each consisting of different cost functions or constraints. For each scenario, a

free final time, fixed final state formulation was used. The variables in the problem are defined below in Table 2.

Table 2 – Optimization Problem Variables

Aircraft Position	x_p, y_p
Forward Sensor Footprint Position	x_s, y_s
Side Sensor Footprint Position	$\overline{x_s}$, $\overline{y_s}$
Aircraft heading/Rate	θ/ω
Time Unit	Δt
Wind Heading	χ
Wind Magnitude	β
States	$z = \{x_p, y_{p,}, \theta\}$
Control	ω for $\lvert 1 \rvert \geq \omega$
Disturbances	χ , β

The vehicle's dynamics are described by the continuous equations of motion shown below in Equations 24 through 26.

$$\dot{x} = V\cos\theta + \beta\cos\chi \tag{24}$$

$$\dot{y} = V\sin\theta + \beta\sin\chi \tag{25}$$

$$\dot{\theta} = \omega \tag{26}$$

Utilizing these equations of motion, the following describes the discretized dynamic optimization process for viewing targets with MAVs equipped with fixed sensors.

3.6.1 Discretization Process

The results of this research are based on a first order Euler discretization of the equations of motion. The first step in the discretization process is to express the equations of motion in parametric form.

$$x(t) = x(t_0) + \int_{t_0}^{t} \dot{x}(t)dt \quad \textbf{(27)}$$

$$y(t) = y(t_0) + \int_{t_0}^{t} \dot{y}(t)dt \quad \textbf{(28)}$$

$$\theta(t) = \theta(t_0) + \int_{t_0}^{t} \dot{\theta}(t)dt \quad \textbf{(29)}$$

By defining a time interval, the state Equations 27 through 29 can be analyzed using discrete time increments. The time interval will be defined as follows.

$$t_0 < t < t_f \quad \textbf{(30)}$$

By dividing the final time into N discrete steps, the time at each step is defined by the following.

$$t_i = t_0 + N * \Delta t \quad \textbf{(31)}$$

Using Equation 31, the system states can now be expressed at any i^{th} time, as defined below.

$$S(i) = \begin{bmatrix} x(i) \\ y(i) \\ \theta(i) \end{bmatrix} \quad \text{for } i = 0,1,2,...,N \quad \textbf{(32)}$$

Now using a first order Euler discretization process, with Equations 27 through 29 in parametric form, the state equations can be expressed.

$$S(i+1) = f(S(i), u(i), \triangle t) = \begin{bmatrix} x(i+1) \\ y(i+1) \\ \theta(i+1) \end{bmatrix} = \begin{bmatrix} x(i) + \dot{x}(i) * \triangle t \\ y(i) + \dot{y}(i) * \triangle t \\ \theta(i) + \dot{\theta}(i) * \triangle t \end{bmatrix} \text{ for } i = 0, 1, 2, ..., N-1 \quad \textbf{(33)}$$

Finally, with the state equations in discrete form, they can be propagated forward in time by optimization software to solve for an optimal solution.

3.6.2 Problem Setup

The objective function, defined below in Equation 34, will be used for the initial set of minimum time results.

$$\min_u J = \phi(x(N), \triangle t) = N \triangle t \quad \textbf{(34)}$$

The state equations that define the dynamics of the system, as well as the initial conditions on those states are described below in Equations 35 through 40.

$$x_p(i+1) = f^x(z(i), u(i), \triangle t) = x_p(i) + \triangle t(V \cos\theta(i) + W_x(i)) \quad \textbf{(35)}$$

$$y_p(i+1) = f^y(z(i), u(i), \triangle t) = y_p(i) + \triangle t(V \sin\theta(i) + W_y(i)) \quad \textbf{(36)}$$

$$\theta(i+1) = f^\theta(z(i), u(i), \triangle t) = \theta(i) + \omega(i) * \triangle t \quad \textbf{(37)}$$

$$0 = x_p(0) - x_{p0} \quad \textbf{(38)}$$

$$0 = y_p(0) - y_{p0} \quad \textbf{(39)}$$

$$0 = \theta(0) - \theta_0 \quad \textbf{(40)}$$

Equations 41 through 43 below describe both the equality and terminal constraints placed on the states. These constraints consider the placement of the forward mounted sensor as well as the final "look angle" of the vehicle.

$$\psi_x(z(N),\triangle t) = (x_{sensor} - x_{target}) \qquad for\ x_{sensor} = (x_p(N+1) + d\cos\theta(N+1)) \quad \textbf{(41)}$$

$$\psi_y(z(N),\triangle t) = (y_{sensor} - y_{target}) \qquad for\ y_{sensor} = (y_p(N+1) + d\sin\theta(N+1)) \quad \textbf{(42)}$$

$$\psi_\theta(z(N),\triangle t) = \theta(N+1) - \theta_f \quad \textbf{(43)}$$

The equations outlined above provide all of the information required to solve the dynamic optimization problem using the optimization software in Matlab.

3.6.3 Necessary Conditions for Optimality

The gradient is calculated in an attempt to solve for an analytical solution. It also can provide useful information regarding the accuracy of the optimization results. Using the state Equations 35 through 37 adjoined with Lagrange multipliers, the Hamiltonian can be formed.

$$\begin{aligned} \mathrm{H}(z(i),u(i),\triangle t) = {} & \lambda^{x\,T}(i+1)[x_p(i) + \triangle t(V\cos\theta(i)) + W_x(i)] + \ldots \\ & \lambda^{y\,T}(i+1)[y_p(i) + \triangle t(V\sin\theta(i) + W_y(i)] + \lambda^{\theta\,T}(i+1)[\theta(i) + \omega(i)\triangle t] \end{aligned} \quad \textbf{(44)}$$

The augmented cost function, Equation 46, can then be formed with the Hamiltonian and the augmented terminal cost shown in Equation 45, which describes the terminal cost adjoined with the terminal constraints.

$$\Phi(z(N),\triangle t) = N\triangle t + \upsilon^{x\,T}[(x_s - x_t)] + \upsilon^{y\,T}[(y_s - y_t)] + \upsilon^{\theta\,T}[(\theta(N+1) - \theta_t)] \quad \textbf{(45)}$$

$$\begin{aligned}\bar{J} = \Phi(z(N),\triangle t) - \lambda^{x^T}(N)x_p(N) - \lambda^{y^T}(N)y_p(N) - \lambda^{\theta^T}(N)\theta(N) + \ldots \\ \lambda^{x^T}(0)x_{p0} + \lambda^{y^T}(N)y_{p0} + \lambda^{\theta^T}(N)\theta_0 + \sum_{i=1}^{N}[H(z(i),u(i),\triangle t) - \ldots \\ \lambda^{x^T}(i)x_p(i) - \lambda^{y^T}(i)y_p(i) - \lambda^{\theta^T}(i)\theta(i)]\end{aligned} \quad \textbf{(46)}$$

The co-states are formed by taking the gradient of the Hamiltonian (44) with respect to each state variable.

$$\lambda^{x^T}(i) = H_x(z(i),u(i),\triangle t) = \lambda^{x^T}(i+1) \quad \textbf{(47)}$$

$$\lambda^{y^T}(i) = H_y(z(i),u(i),\triangle t) = \lambda^{y^T}(i+1) \quad \textbf{(48)}$$

$$\begin{aligned}\lambda^{\theta^T}(i) = H_\theta(z(i),u(i),\triangle t) = -\lambda^{x^T}(i+1)\triangle tV\sin\theta(i) + \ldots \\ \lambda^{y^T}(i+1)\triangle tV\cos\theta(i) + \lambda^{\theta^T}(i+1)\end{aligned} \quad \textbf{(49)}$$

The final co-states are formed by taking the gradient of the augmented terminal cost Φ (45) with respect to each state variable.

$$\lambda^{x^T}(N) = \Phi_x(z(N),\triangle t) = \upsilon^x \quad \textbf{(50)}$$

$$\lambda^{y^T}(N) = \Phi_y(z(N),\triangle t) = \upsilon^y \quad \textbf{(51)}$$

$$\lambda^{\theta^T}(N) = \Phi_\theta(z(N),\triangle t) = -\lambda^x(i)d\sin\theta(N+1) + \lambda^y(i)\cos\theta(N+1) + \upsilon^\theta \quad \textbf{(52)}$$

The optimality criterion is now expressed as the gradient of the Hamiltonian (44) with respect to the control, $u(i)$.

$$\mathrm{H}_u(\mathrm{z}(i),u(i),\triangle t) = \lambda^{\theta^T}(i+1)\triangle t = 0 \quad \textbf{(53)}$$

Finally, since we are solving a minimum time problem, the transversality criterion is needed to solve for the additional $\triangle t$ variable. This equation is found by adding Equations 44 and 45 and taking the gradient with respect to the time step, which gives,

$$N + \sum_{i=1}^{N} [\lambda^{x^T}(i+1)[V\cos\theta(i) + W_x] + \lambda^{y^T}(i+1)[V\sin\theta(i) + W_y] + \ldots \\ \lambda^{\theta^T}(i+1)[\omega(i)]] = 0 \quad (54)$$

Utilizing these equations, the co-states of Equations 47 through 49 can be solved starting with estimated values of the final co-state from Equations 50 through 52. Additionally, the state equations can be solved starting with the initial conditions to the states.

3.7 Flight Path Variations

This research considered three different flight path variations. The first path determined consists of the minimum time for the aircraft to get from an initial point and heading to a final point and heading with a constrained turn radius. The second path evaluates the scenario of an aircraft flying between two buildings, where the vehicle's turn radius is larger than the corridor in which it needs to fly. The final case utilizes both the forward mounted sensor as well as the side mounted sensor to find a stationary target in a minimum time fashion, and then continually tracks that target for any duration of time.

3.7.1 Minimum Flight Time with Forward Sensor

The minimum time flight path consisted of flying an aircraft from an initial point and heading to a final point and heading utilizing the forward mounted sensor. For this scenario, the Dubins path simulation, described in Section 3.5, provides a very realistic initial guess to the optimization software. This allows for the optimization software to iterate on a good solution until it finds the best solution possible. In total, three simulations were run to determine the robustness of the model. Based on an initial set of

conditions, the final target viewing angle and the heading of the wind were individually varied from 0 – 360 degrees in five-degree increments. Additionally, the aircraft was required to always take-off into the wind. Therefore, as the wind direction varied, the initial heading of the vehicle was varied as well. The magnitude of the wind, β, was also varied from 0 to 70% in 2% increments.

The dynamic optimization setup for this problem is the same as outlined in the problem setup of Section 3.6.2.

3.7.2 Minimum Flight Time with Side Sensor

This minimum time flight path consisted of flying an aircraft from an initial position and heading to a final position, regardless of the final heading, utilizing only the side sensor of the MAV. One of the concerns of target tacking is that once a target is found, it may have to be monitored for an extended duration of time. There are two methodologies for accomplishing this task. The first method is to find the target with the forward mounted sensor in minimum time fashion, then transition to the side sensor along an orbital track. The concern with this method is the target will not be monitored during the transition period. The second method is to utilize only the side sensor. Therefore, once the sensor is placed on the target, the vehicle will be in position to follow an orbital track, and no transition will be required. As a result, the target will be monitored continually throughout the flight path. To evaluate these two methodologies, the minimum flight time using only the forward sensor and the minimum flight time using only the side sensor will be compared.

To accomplish this dynamic optimization, a path estimation needed to be developed for utilizing the side sensor. In order for the footprint of the side sensor to be placed on the target, the vehicle will be required to fly to a point on a circle around the target of radius d_E, with a heading vector tangent to that circle. Therefore, the Dubins path methodology was utilized to determine the shortest path from the initial conditions to a point and heading on this circle. This path was then implemented into the optimization software as the initial guess to the system. The optimization procedure for this simulation are the exact same as those utilized for the forward sensor simulation detailed above in Section 3.7.1, with the exception of the constraints placed on the states. For both the forward sensor and side sensor flight paths, the final heading constraints will be omitted. Additionally, the constraints for the side sensors flight path will be replaced with Equations 55 and 56 below. These two equations express the difference in the position of the footprint of the side sensor with the position of the target.

$$\psi_x(z(N),\Delta t) = (\bar{x}_{sensor} - x_{target}) \quad for\ \bar{x}_{sensor} = x_p(N+1) + d\cos(\theta(N+1) + \pi/2) \quad \textbf{(55)}$$

$$\psi_y(z(N),\Delta t) = (\bar{y}_{sensor} - y_{target}) \quad for\ \bar{y}_{sensor} = y_p(N+1) + d\sin(\theta(N+1) + \pi/2) \quad \textbf{(56)}$$

3.7.3 Flight Path through an Urban Canyon

The next phase of the research was to consider flight through an urban canyon. In the previous results, the shortest flight path was found based on the vehicles minimum radius turn. However, in an urban canyon, the vehicle may be required to fly between buildings where there may not be enough distance for a minimum radius turn. In other words, if the vehicle flew the profile above, it may fly into the side of a building and be destroyed.

Therefore, the objective was to fly in a straight line to the target. When the aircraft approaches the final position, it will adjust to put the sensor footprint over the target at the desired angle. For this scenario a new cost function was implemented; however, the Dubins path, as developed for the first model, will no longer give an accurate initial guess to the problem and therefore must be augmented to estimate the optimal path. This augmented path consists of an initial Dubins path to get the aircraft on the straight line solution. Once on that line, the aircraft maintains a constant heading until it comes within close proximity of the target. At this point, a second Dubins path is flown to put the sensor footprint on that target.

The new cost function for this scenario is described below in Equation 57. The remainder of the optimization problem is the same as described in the problem setup of section 3.6.2.

$$\min_u J = \phi(x(N)) = N\triangle t + \sum_{i=1}^{N} (\frac{y(i)}{x(i)} - \frac{y_f}{x_f})^2 \quad \textbf{(57)}$$

This new cost function consists of a minimum time terminal cost, as well as a path cost that encourages the optimization to keep the flight path at a constant angle. First, the current flight angle of the aircraft is calculated. This angle is then subtracted by the final angle and that quantity is squared. This process is described below in Figure 14 by minimizing the error between $\phi_{Current}$ and ϕ_{Final}. By minimizing the deviation of these angles, the aircraft will fly the straight-line path to the final position. The problem formulation postpones maneuvering to obtain the required final heading until it cannot be postponed anymore and still view the target with the specified viewing angle.

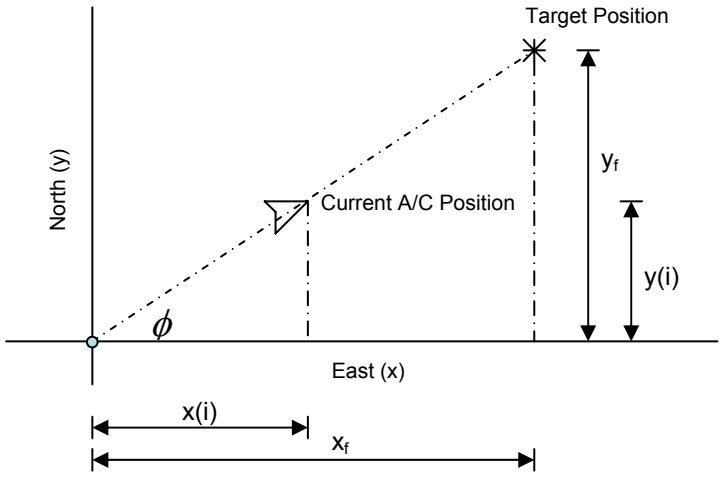

Figure 14 - MAV Flight Angle Characterization

$$\phi_{Current} = y(i) / x(i) \tag{58}$$

$$\phi_{Final} = y_f / x_f \tag{59}$$

3.7.4 Continuous Tracking for Dual Sensors

Now, consider the case where the stationary target needs to be viewed from all angles, or the target needs to be monitored for some duration of time. This can be accomplished by using the side sensor of the vehicle, which is mounted at a 30-degree angle to the vertical as described previously in Figure 6. The vehicle will find the target similar to the methods described above using the forward mounted sensor. Once it has acquired the target, the vehicle will transition into an orbital pattern to continuously view the target with its side mounted sensor, while accounting for a constant wind.

For this research, only a point mass model is utilized. Therefore, as the aircraft begins to fly its orbit, it will not bank, but will fly its orbit keeping wings level. This will keep the sensor footprint a fixed distance from the aircraft.

To accomplish this scenario, the optimization was broken into three separate phases. In the first phase, the vehicle used its forward mounted sensor to view the target as quickly as possible without requiring a desired viewing angle. As soon as the target was in sight with the forward mounted sensor, the vehicle adjusted its flight path such that the side-mounted sensor was placed on the target, again in minimal time. This is accomplished in the transition stage where, for a sensor mounted out the left side of the vehicle, it is optimum for the vehicle to fly a partial right turn. This would put the aircraft on a pseudo circular orbit such that the time the side sensor is fixed on the target is optimized.

The initial flight path consisted of the same problem setup as discussed above in Section 3.6.2 with one exception. Since there is no requirement for the final target viewing angle, the final heading constraint of Equation 40 will not be implemented. This allows the vehicle to put its sensor on the target as quickly as possible.

The second flight path will have the same minimum time cost function; however, the sensor constraints placed on the system will utilize the side sensor. The constraints implemented for this path are the same as the minimum time side sensor constraints expressed in Equations 55 and 56.

The final flight path will no longer exploit a minimum time cost function. The new cost function consisted of a path cost that will require the sensor footprint to remain on the target throughout the flight. This cost function is described below in Equation 60.

$$\min_{u} J = \phi(x(N)) = \sum_{i=1}^{N} \left[(\bar{x}_s(i) - x_f)^2 + (\bar{y}_s(i) - y_f)^2 \right] \quad \textbf{(60)}$$

Additionally, a new constraint is added to give a terminal condition to the simulation. In this case, the orbital path is broken into four sections. Therefore, this path will need to be run four times to complete the final flight path. The constraints that must be satisfied for this scenario are Equations 55, 56 and an additional constraint to provide a final required heading for the vehicle, described below in Equation 61.

$$\psi_y(\theta(N), \Delta t) = \theta(N+1) - (\theta(1) - \pi/2) \quad \textbf{(61)}$$

Combining these four paths will result in the optimum flight path for viewing targets with dual sensors in a constant wind under these constraints.

3.8 Chapter Summary

This chapter provided the fundamental equations and parameters required for the three different optimization scenarios. With the optimization equations defined, and an adequate initial guess for the solution with the Dubins path, the Matlab optimization toolbox was used for optimal flight path planning.

4. Test Results and Analysis

4.1 Overview

Chapter 4 presents the results of the research conducted for this thesis. Section 4.2 presents the path planning for the minimum time scenario. This includes the Dubins path that is used as the initial guess for the optimization software. The plots of the Dubins path depict both the air path and ground path of the vehicle as well as the position of the sensor and target at each time step. The optimized flight path only shows the ground path of the vehicle but does include the sensor and target positions. Section 4.2 is followed by an analytical solution to the minimum time problem which provides valuable information that shows the accuracy of the numerical solution. This is followed by path planning results for both the urban canyon scenario as well as the dual sensor scenario.

4.2 Minimum Flight Time with Forward Sensor Results

The results for the dynamic optimization are based on an initial set of parameters. These parameters, shown below in Table 3, were chosen as the base case for this scenario and will be referred to throughout this section

Table 3 - Initial Parameters for the Minimum Time Scenario

Start Position	(0,0)	Final Position	(30,0)
Initial heading	90^o	Final Heading	180^o
Wind Magnitude, β	0.4	Wind Direction, χ	270^o

This scenario utilizes Dubins Path as an initial guess for the simulation software. Figure 15 below shows the Dubins path as well as the time calculated to fly that path. The process to develop this plot is as described in Section 3.5.

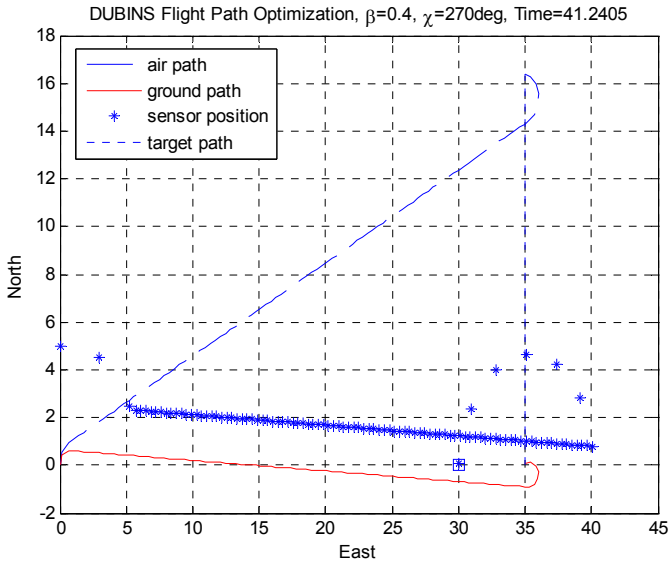

Figure 15 - Dubins Flight Path for Min Time Solution

The control for this flight path is input into the dynamic optimization as an initial guess for the optimal solution. The final optimized flight path is shown below in Figure 16. Again, the sensor footprint is represented by the asterisk, the target position is displayed as a square at position $(30, 0)$, and the arrow vectors indicate the vehicles heading.

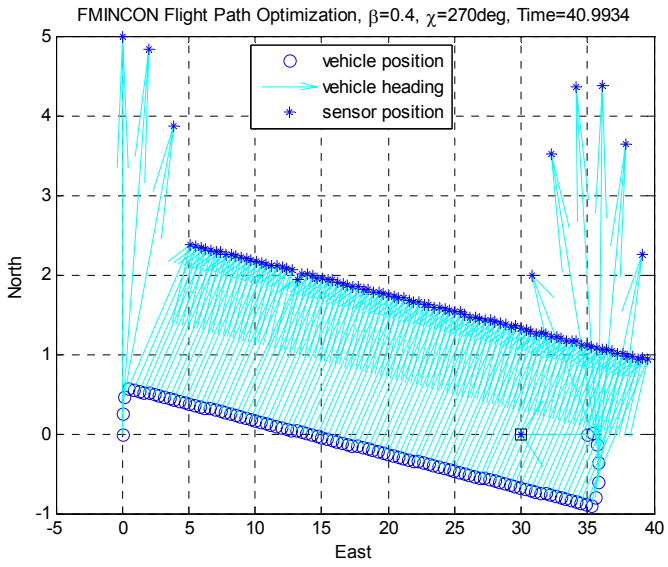

Figure 16 - Optimized Flight Path for Min Time Solution

This shows an optimal flight path for the given scenario. By varying critical parameters to the flight path, the robustness of the optimization algorithm is tested. The first case considered wind headings over a 360-degree spectrum. For the scenario, the vehicle will always be required to take-off with an initial heading directly into the wind. Therefore as the wind heading is varied over 360-degrees, the initial heading will also be varied. The results show a smooth surface plot, as seen in Figure 17A, which describes the flight time against the vehicles heading over the range of the wind heading. Figure 17(B – D) will describe each face of this surface plot. Figure 17B shows the flight time compared to the changing winds, which show a maximum flight time when there is a direct head wind, and min flight time when there is direct tail wind. Figure 17C shows the vehicle's heading compared to the changing winds. This proves accurate, showing the aircraft's heading varies drastically based on whether the wind approaches from the right or left side of the aircraft. Finally, Figure 17D shows the relationship of the

vehicles heading to the time of flight. This gives an indication of omega, ω, which again is the change in heading over the course of the flight and is used as the control to the system.

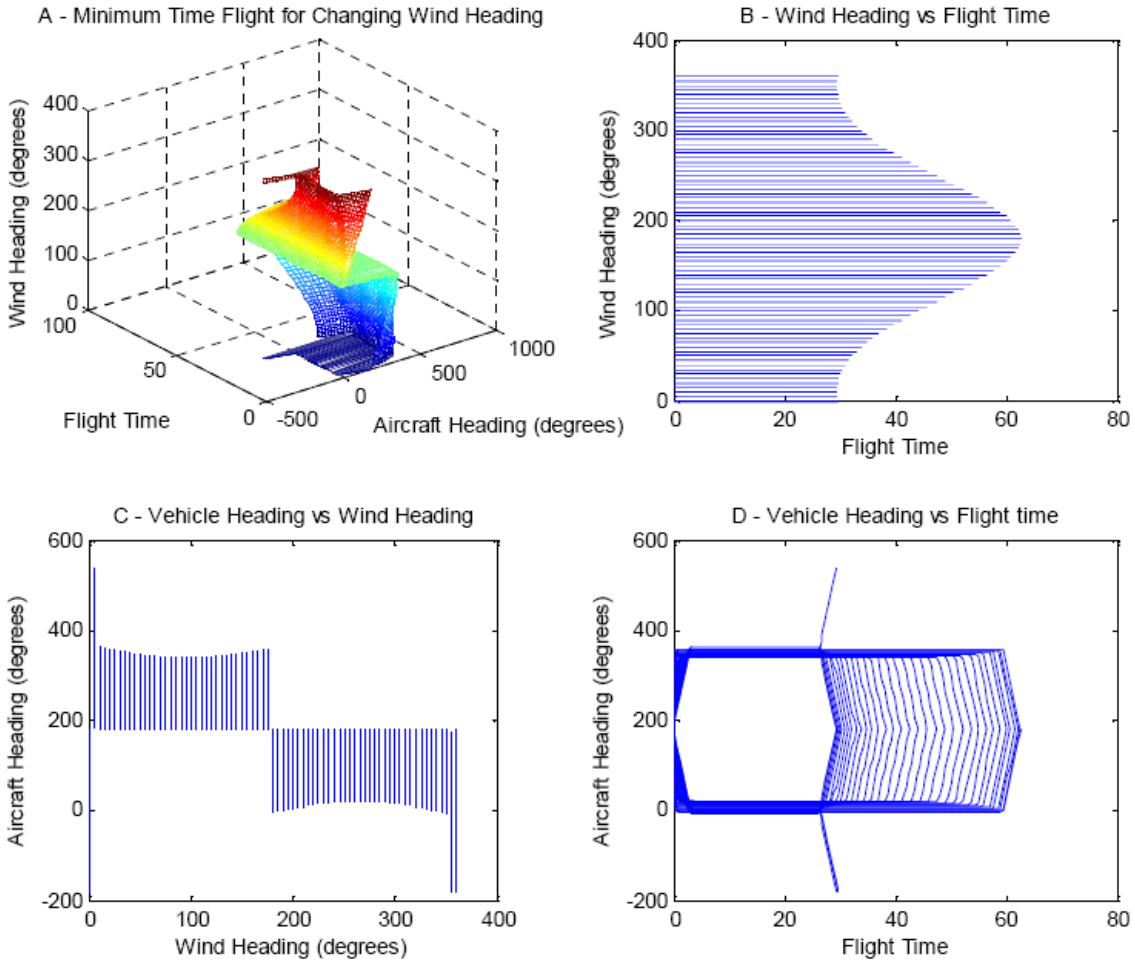

Figure 17 - Surface Plots - Varying Wind Heading with the Min Time Scenario

To aid in the comprehension of Figure 17, Figures B,C, and D are shown again for specific wind values. This gives an indication of exactly what is occurring over the course of a flight. The following plots describe a flight path for winds at 45, 135, 225, and 315 degrees. This is just four of the seventy-two individual occurrences that are shown above in Figure 17. Figure 18 below takes a closer look at Figure 17B, which

considers the wind heading verses the path flight time. This plot verifies that the time of flight will increase as an increasing head wind acts on the vehicle.

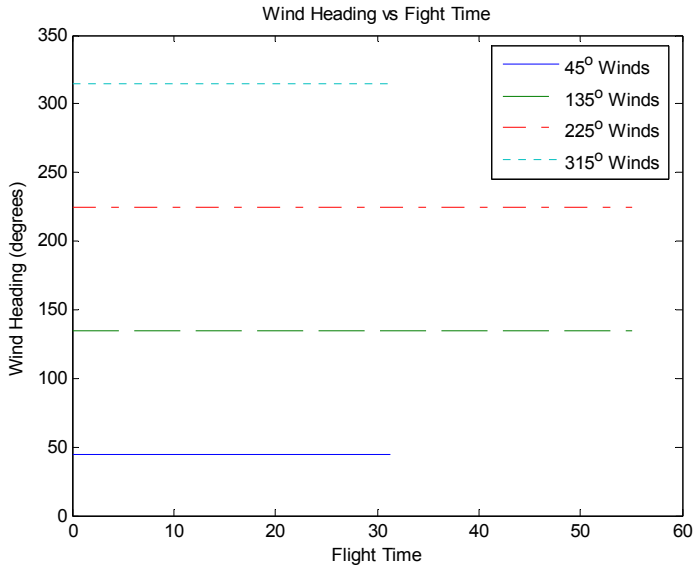

Figure 18 - Min Time Wind Heading vs Flight Time; Varied Wind Heading

In evaluating Figure 17C, the same four wind values are shown to describe the aircraft's heading verses the wind heading. This is shown below in Figure 19 and describes the range of the vehicle's headings used throughout the flight path. This plot gives an indication of whether the vehicle flies north or south of the target.

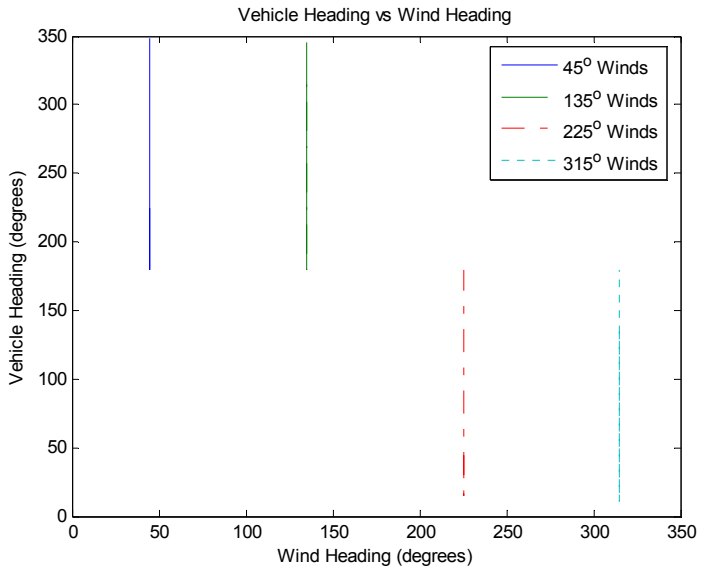

Figure 19 - Min Time Aircraft Heading vs Wind Heading; Varied Wind Heading

Finally in evaluating Figure 17D, the same four wind values are shown to describe the aircraft heading verses the wind heading. This is shown below in Figure 20. This plot verifies that after the aircraft adjusts from its initial heading, and before it accounts for the final target viewing angle, the aircraft's heading is constant, as it is accounting for the constant wind. It also gives an indication of the turn rate that is required by the vehicle. Additionally, it can be seen that the initial heading is changing, based on the wind direction.

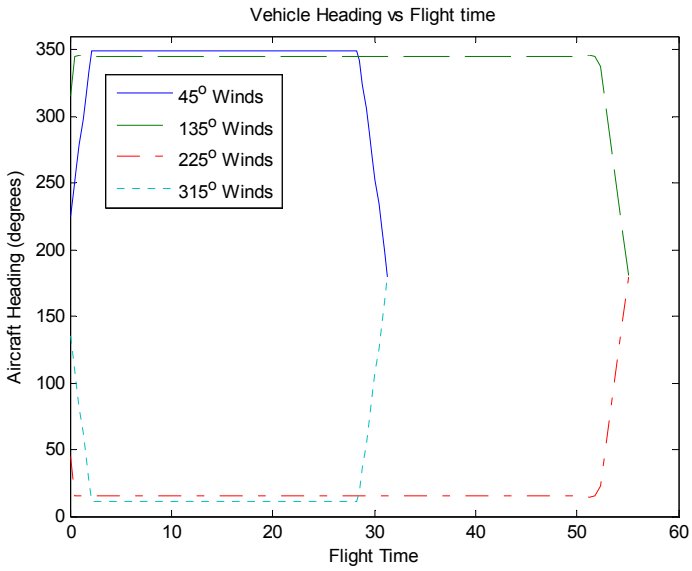

Figure 20 - Min Time Aircraft Heading vs Flight Time; Varied Wind Heading

The second case evaluated the change in the final viewing angle of the target over a 360-degree spectrum per the base case. Here Figure 21(A – D) is described in the same manner as above in Figure 17. Figure 21A shows a smooth surface plot across the range of target-viewing angles. Figure 21B describes the flight time as the target-viewing angle is varied. The aircraft heading compared to the target-viewing angle is shown in Figure 21C. Finally, the rate of change of the vehicles heading is shown in Figure 21D.

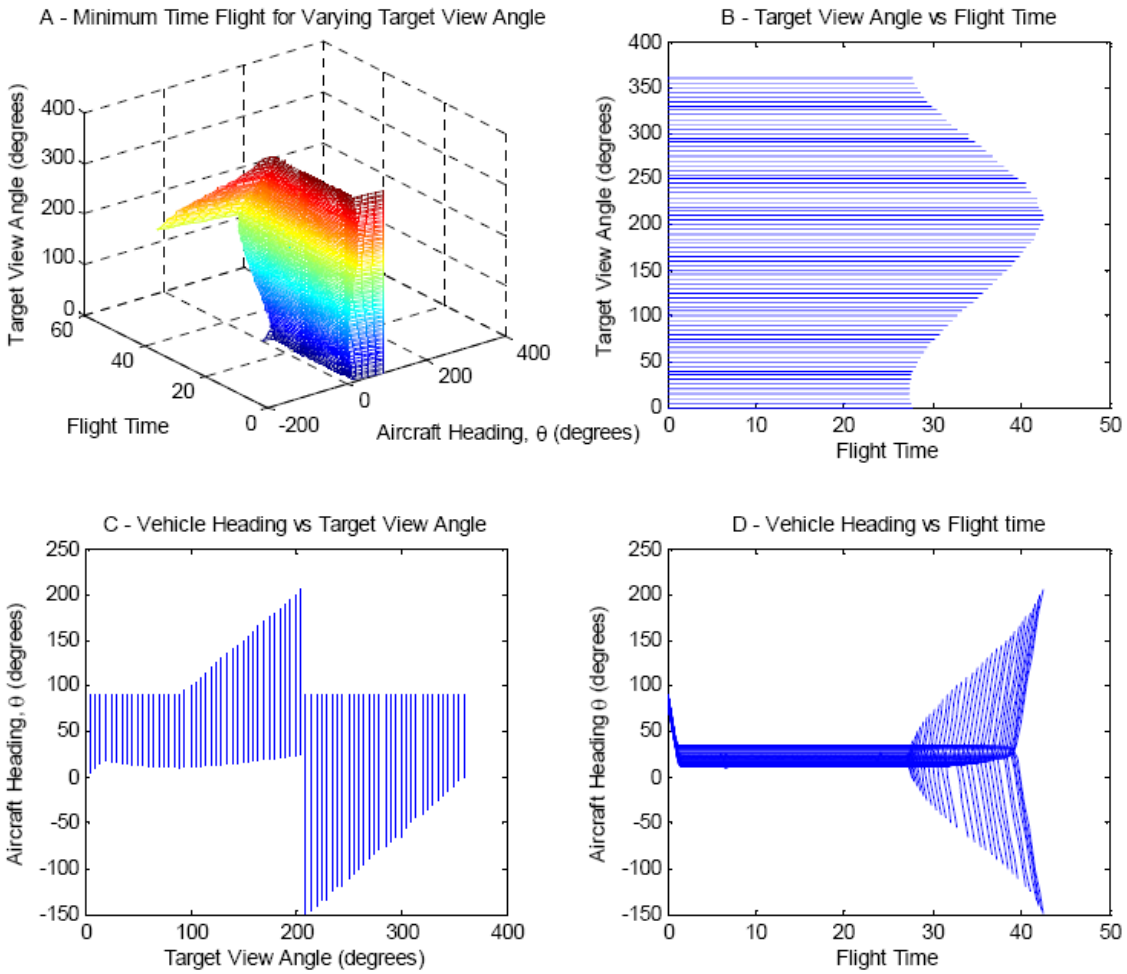

Figure 21 - Surface Plots - Varying Final Heading with the Min Time Scenario

Again, a better understanding of Figure 21 can be achieved by evaluating plots B through D, which describe each face of the surface. For each of these cases, the following four different target viewing angles will be viewed; 45 degrees, 135 degrees, 225 degrees, and 315 degrees. Below in Figure 22, the target-viewing angle is plotted against the total time of the flight path. This shows that the longest flight time will occur for when the aircraft is required to view the target at 180 degrees opposite for which it approaches the target.

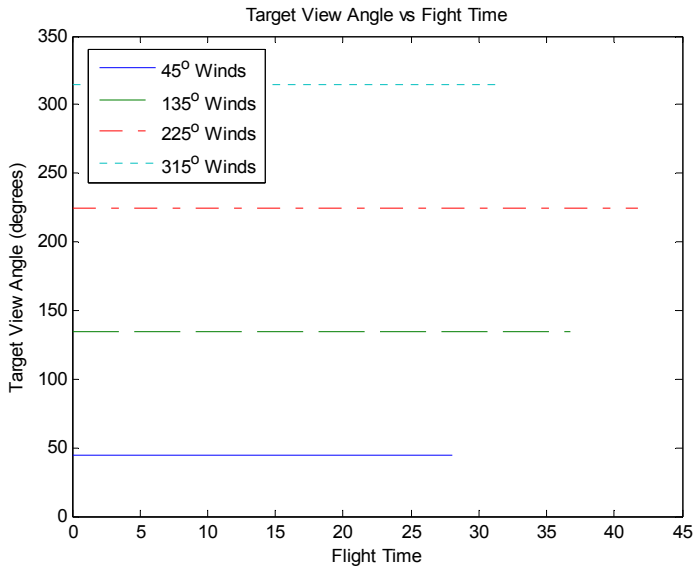

Figure 22 - Min Time Target View Angle vs Flight Time; Varied Target Angle

Next, the aircraft's heading is plotted against the target-viewing angle. The four chosen viewing angles are shown below in Figure 23. This is a subset of Figure 21C and describes the range of headings that is required for the aircraft to complete the simulation.

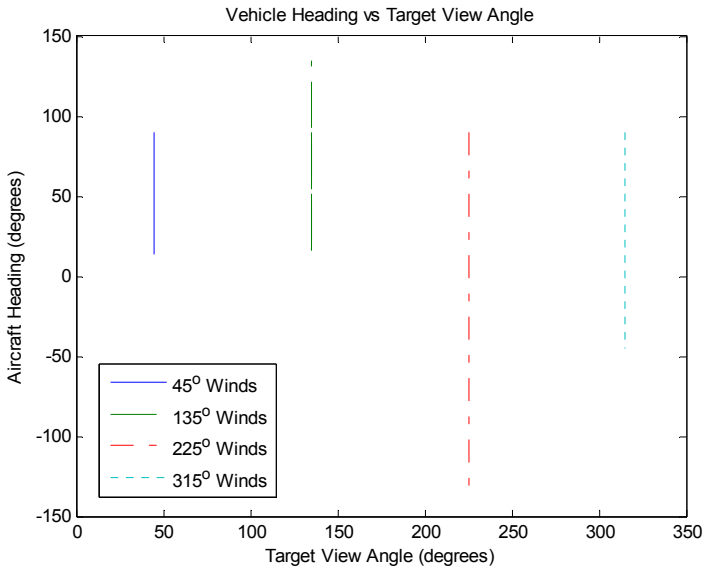

Figure 23 - Min Time Aircraft Heading vs Target View Angle; Varied Target Angle

Finally, the aircraft's heading is plotted against the flight time and is shown in Figure 24. Again, this depicts the heading rate of the aircraft as well as the crab angle required to offset the wind. This is a subset of Figure 21D.

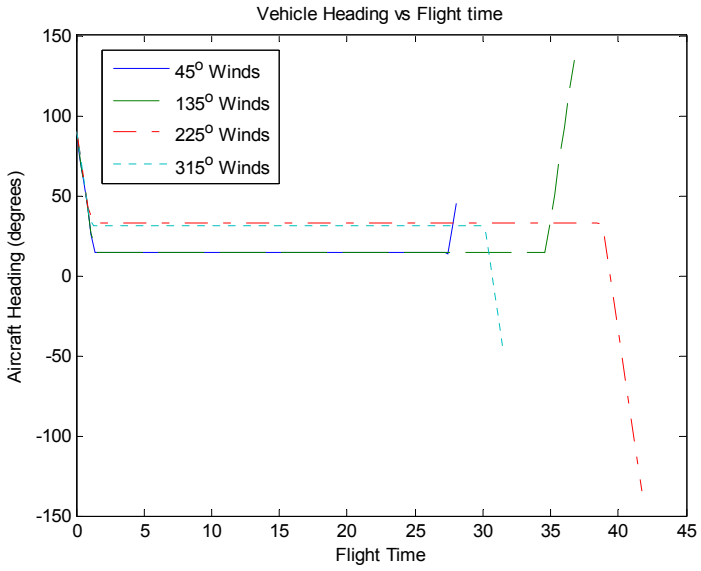

Figure 24 - Min Time Vehicle Heading vs Flight Time; Varied Target Angle

The final case evaluates the change in the magnitude of the wind per the base case. Here the wind to aircraft ratio is varied from zero wind to seventy percent wind. This case is shown below in Figure 25(A-D). Figure 25A shows a relatively smooth surface plot for a varied wind magnitude. Slight perturbations to the optimal flight paths can be seen as the wind magnitude reaches seventy percent of the MAVs speed. Figure 25B describes the flight time as the wind magnitude increases. Figure 25C evaluates the vehicle's heading for changing wind magnitudes. Figure 25D describes the rate of change of the MAVs heading over the course of the flight.

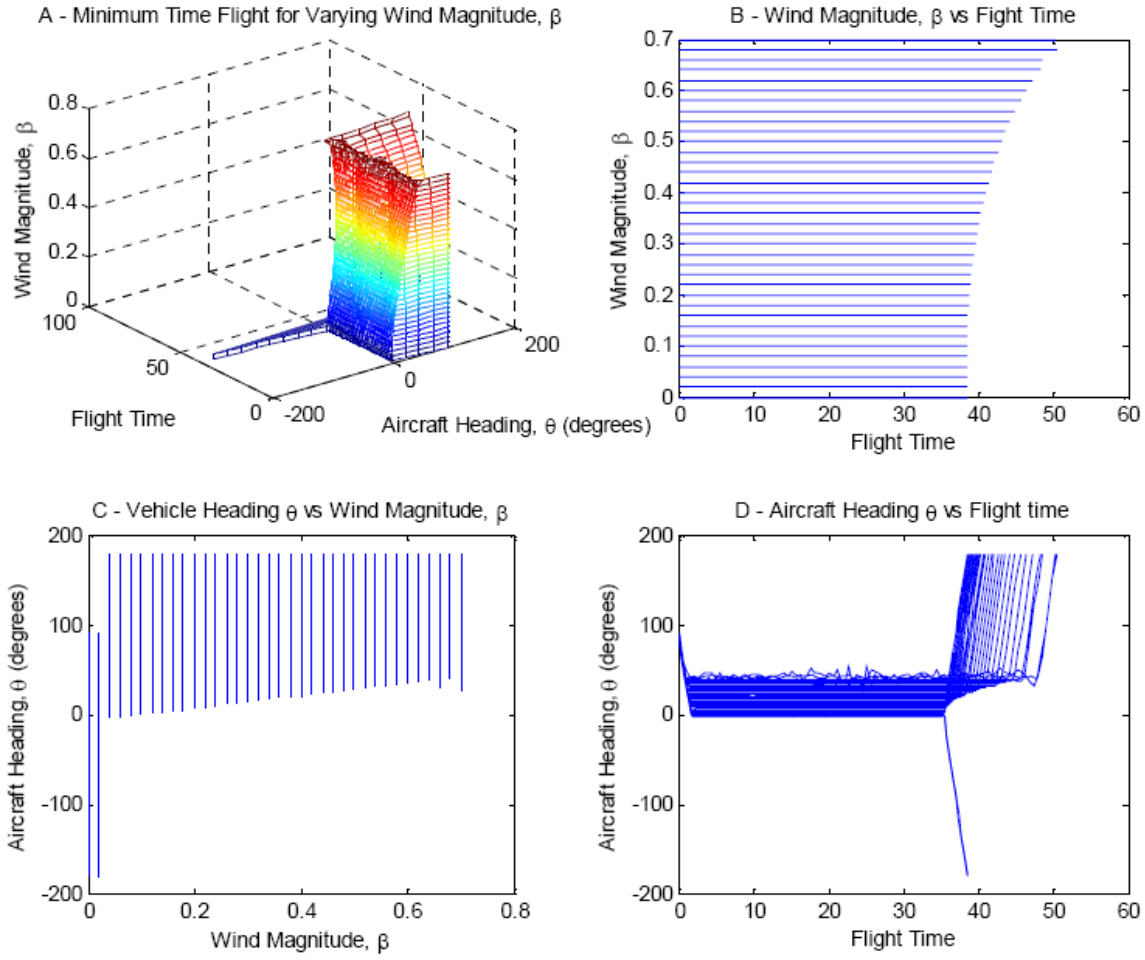

Figure 25 - Surface Plots - Varying Wind Speed with the Min Time Scenario

Plots B through D are again shown in more detail by evaluating four separate cases. The wind will be shown below at 14%, 28%, 42%, and 56%. The first plot evaluated compares the wind speed against the flight time. This is shown below in Figure 26, and proves to be accurate, showing the time of flight increases as a stronger wind is applied to the MAV. This requires a greater crab angle to accurately reach the target, which ultimately increases the total flight time.

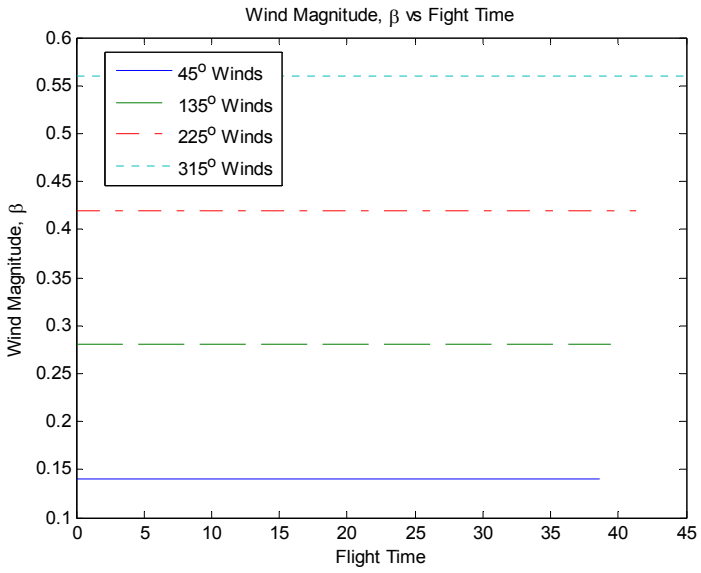

Figure 26 - Min Time Wind Magnitude vs Flight Time; Varied Wind Speed

The next figure evaluates the aircraft's heading against the wind magnitude. This is shown below in Figure 27, which shows very little change in the range of the MAVs heading based on changing wind magnitudes.

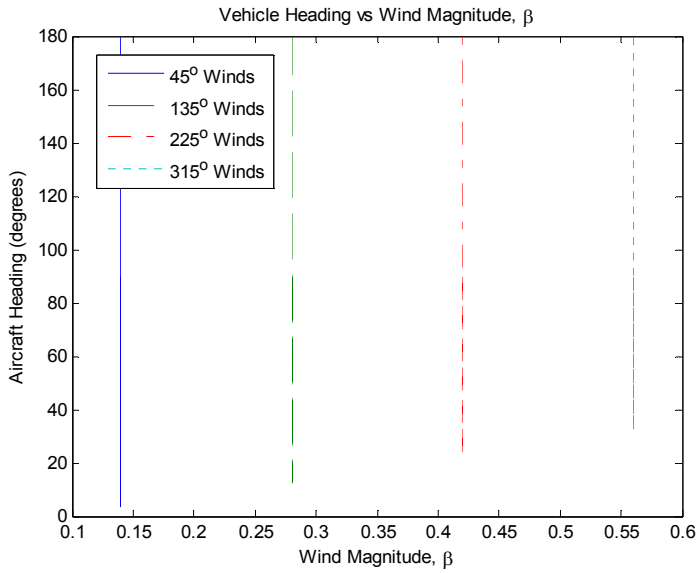

Figure 27 - Min Time Vehicle Heading vs Wind Magnitude; Varied Wind Speed

Finally, Figure 28 below describes the aircraft's heading to the flight time per changing wind magnitude. This plot shows that as the wind continues to grow stronger in magnitude, the vehicle's heading must adjust to remain on the desired flight path.

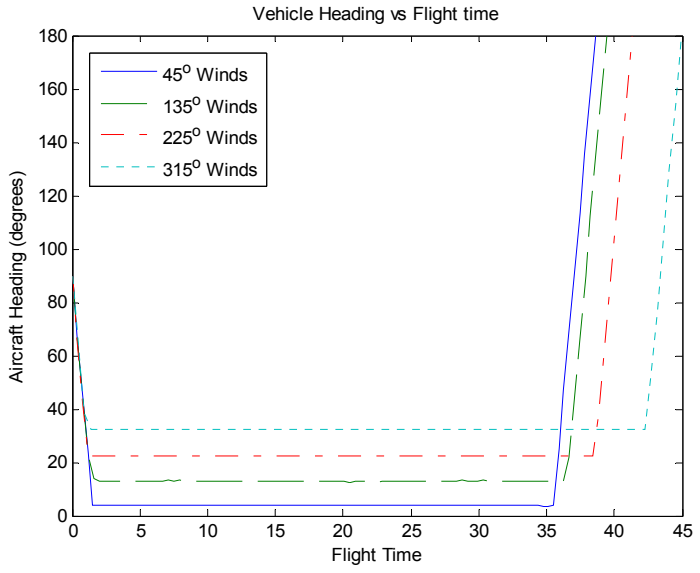

Figure 28 - Min Time Vehicle Heading vs Flight Time; Varied Wind Speed

Each of these cases proves the accuracy and the robustness of the results. It is shown that with a good guess provided by the Dubins path, an accurate solution can be found for the optimal flight path.

4.3 Minimum Time Flight with Side Sensor Results

The results for this section compare the minimum flight time of a MAV when using either a forward mounted sensor or a side mounted sensor.

4.3.1 Flight Path Estimation

A Dubins path was used to give an estimation of the optimal flight path to the optimization software. When considering the optimal flight with the forward mounted sensor, the Dubins path is determined using the same procedures as discussed in section 3.5. However, when the side mounted sensor is utilized, that path is no longer adequate. For this case, the aircraft is required to start at an initial position and heading and fly to a circle around the target with a heading vector tangent to that circle. The radius of the circle must equal d_E, which has been defined previously as the distance the footprint of the side sensor appears next to the aircraft. With these conditions satisfied, the sensor footprint will directly line up with the target. A Dubins path was calculated for numerous points on this circle. This procedure is shown below in Figure 29.

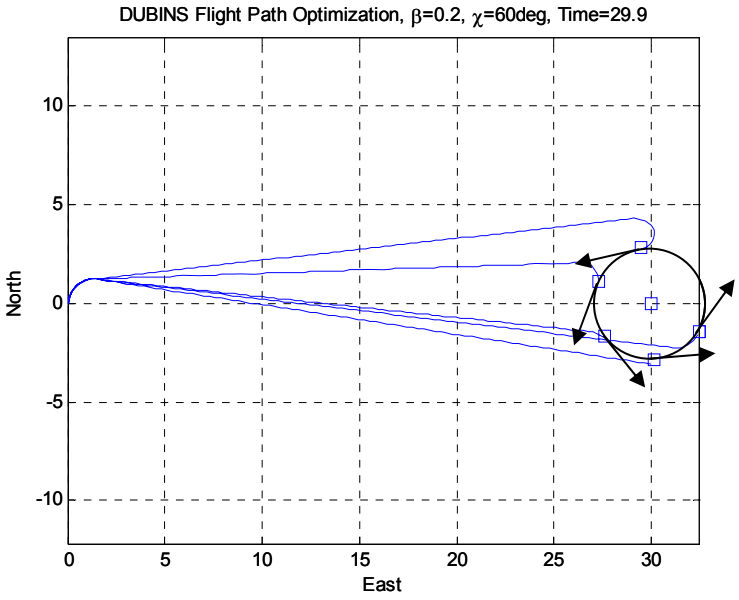

Figure 29 - Iteration of Dubins Path for Side Sensor

Choosing the shortest of these paths, the final path estimation is shown below in Figure 30, and is then used as the initial flight path estimation into the optimization software. This plot shows a sensor footprint distance equal to zero, the path of the virtual target, and both the ground and air path of the vehicle.

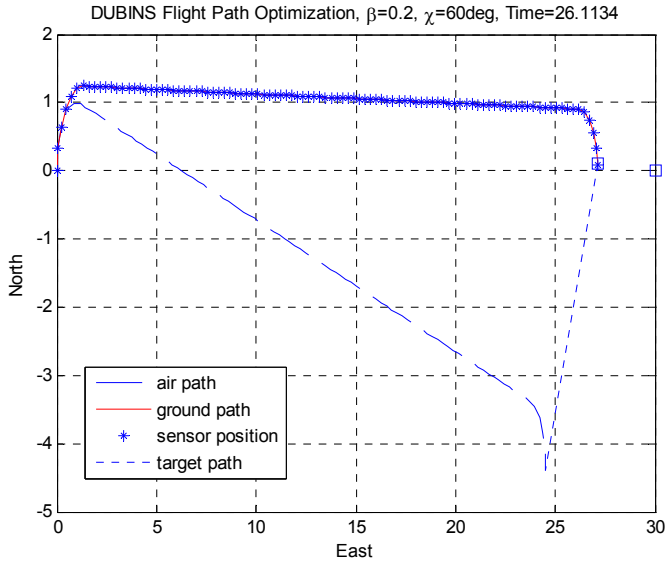

Figure 30 - Minimum Time Path for Dubins Estimation with Side Sensor

4.3.2 Optimization Results

The objective of this scenario is to compare the minimum flight time using the forward sensor against the minimum flight time using the side sensor. This simulation was run for three different sets of parameters, each adjusting the values for both the wind magnitude and heading. These parameters are expressed below in Table 4.

Table 4 - Parameters to Compare Forward and Side Sensor

Start Position	(0,0)	Final Position	(30,0)
Initial heading	χ - 180^o	Final Heading	no constraint
Wind Magnitude, β	0, 0.2, 0.5	Wind Direction, χ	0^o, 180^o, 270^o

The figures below describe the flight paths using both the forward mounted sensor and the side mounted sensor given the parameters expressed in Table 4. The sensor footprint is depicted in each figure as the asterisk, the target position is shown as square located at position $(30,0)$, and the arrows show the heading of the aircraft. The first set of plots, shown below in Figure 31, depict a wind heading of zero-degrees and wind magnitude of 50 percent of the aircraft velocity for the forward mounted sensor and the side mounted sensor respectively.

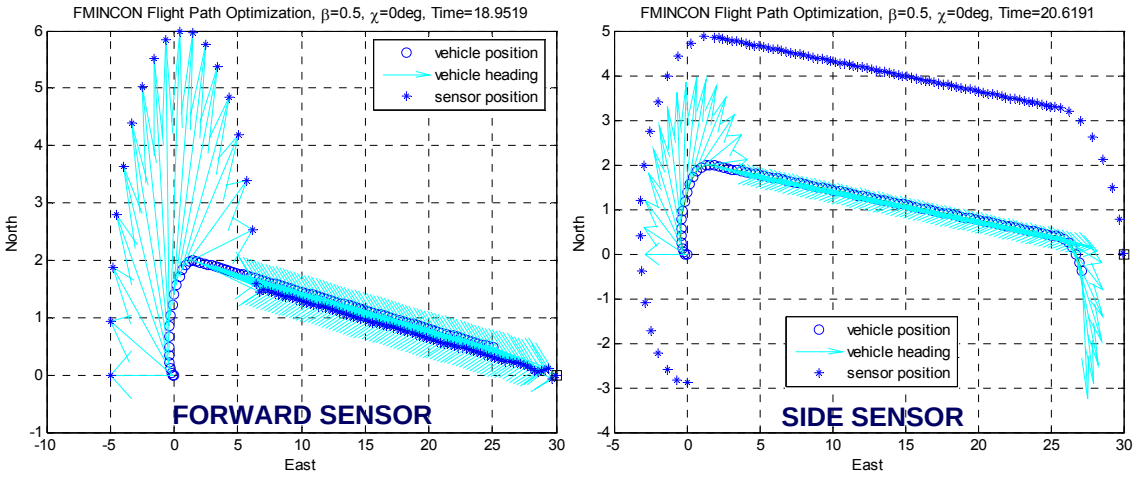

Figure 31 - Minimum Time Flight for Forward and Side Sensors, $\chi = 0$, $\beta = 0.5$

The second set of plots, shown below in Figure 32, depict a wind heading of 180-degrees and wind magnitude of 50 percent of the aircraft's velocity for the forward mounted sensor and the side mounted sensor respectively.

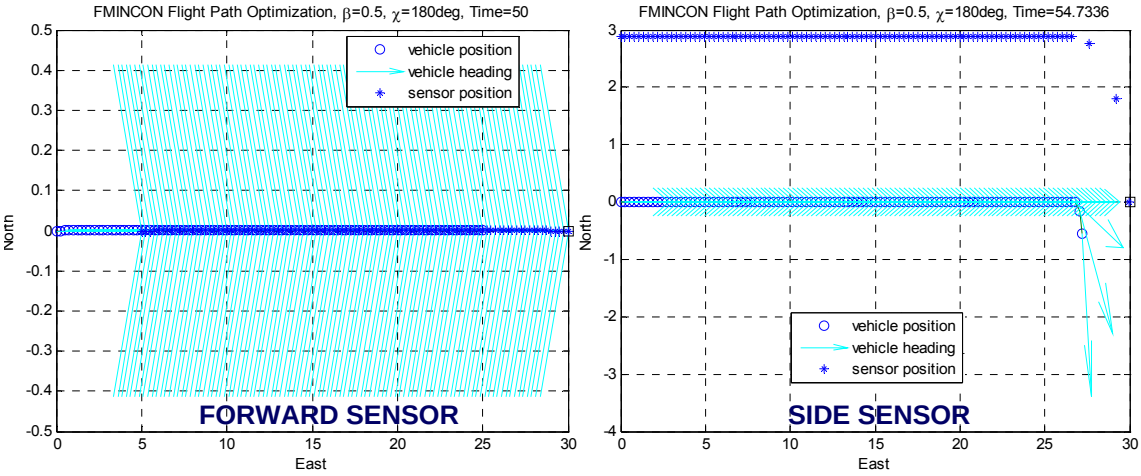

Figure 32 - Minimum Time Flight for Forward and Side Sensors, $\chi = 180$, $\beta = 0.5$

The third set of plots, shown below in Figure 33, depict an initial heading of 270-degrees and wind magnitude of 50 percent of the aircraft's velocity for the forward mounted sensor and the side mounted sensor respectively.

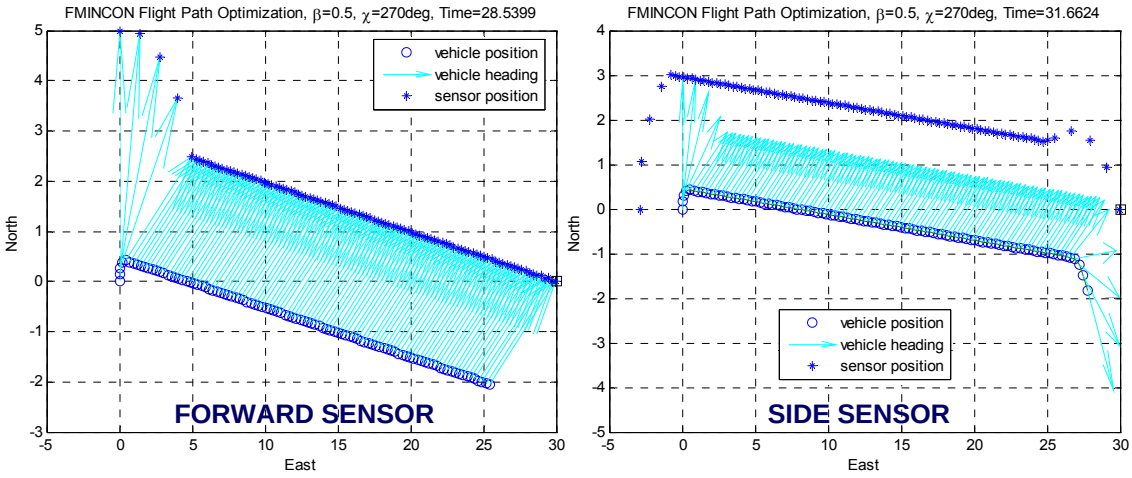

Figure 33 - Minimum Time Flight for Forward and Side Sensors, $\chi = 270$, $\beta = 0.5$

Finally, the results from these parameters are summarized below in Table 5. The difference of the flight times are calculated and shown as the delta, which describes the additional time required for the footprint of the side sensor to be placed on the target.

Table 5 - Forward Sensor vs Side Sensor Flight Time Results

χ (deg)	β	Time Units for Forward Sensor	Time Units for Side Sensor	Δ
0°	0	28.4922	30.9612	2.469
0°	0.2	23.7143	25.7843	2.07
0°	0.5	18.9518	20.6191	1.6673
180°	0	25	27.4566	2.4566
180°	0.2	31.25	34.2917	3.0417
180°	0.5	50	54.7336	4.7336
270°	0	25.7268	28.1952	2.4684
270°	0.2	25.9898	28.5294	2.5396
270°	0.5	28.5399	31.6624	3.1225

These results show that over a wide range of flight parameters, the difference between the flight times when using the forward mounted sensor verses the side mounted sensor can become quite substantial. This may or may not be of significance based on the dimensions of the problem or the situation upon which the vehicle is being used. However it does provide a tool to compare the utility of the forward and side mounted sensors.

4.4 Minimum Time Analytical Solution

An analytical solution is desired for a few reasons. First, it solidifies the results obtained using numerical optimization. Second, it can lead to the development of a control law to be implemented with a flight auto-pilot.

Evaluating the co-state Equations 47 and 48, it is seen that $\lambda^x(i)$ and $\lambda^y(i)$ will remain constant throughout the flight profile, and additionally will equal the Lagrange multipliers of the final co-states expressed in Equations 50 and 51. The optimality criterion shows that $\lambda^\theta(i)$ must equal zero. Therefore the aircraft heading can now be expressed in terms of the co-states as shown below.

$$\tan\theta = \frac{\lambda^y(i+1)}{\lambda^x(i+1)} = \frac{\upsilon^y}{\upsilon^x} \tag{62}$$

Equation 62 proves that the aircraft heading, θ, will be constant throughout the flight profile. With that being known, the transversality criterion can now be used in conjunction with Equation 62 to determine υ^x and υ^y in terms of θ.

$$\upsilon^x = \frac{-1}{V * \cos\theta + W_x + \tan\theta * V * \sin\theta + \tan\theta * W_y} \quad \textbf{(63)}$$

$$\upsilon^y = \frac{-\tan\theta}{V * \cos\theta + W_x + \tan\theta * V * \sin\theta + \tan\theta * W_y} \quad \textbf{(64)}$$

Utilizing Equations 63 and 64 along with the final co-state equation for λ^θ, the Lagrange multiplier υ^θ can be solved. This is expressed below in Equation 65.

$$\upsilon^\theta = \upsilon^x d \sin\theta(N+1) - \upsilon^y d \cos\theta(N+1) \quad \textbf{(65)}$$

Equations 63 through 65 are expressed in terms of the constant flight angle. Given a value for this heading angle, the Lagrange multipliers of the final co-states can be calculated. The values of the Lagrange multipliers were chosen to be solved for because these values can be attained both from the analytical solution described above as well as from the output of the numerical solution. However, to achieve consistent results, the constraint placed on the turn rate ω must be omitted from the numerical solution since the analytical solution does not account for this constraint. Additionally, there will be no constraint placed on the initial heading of the aircraft. Given these conditions, the optimal path is shown below in Figure 34.

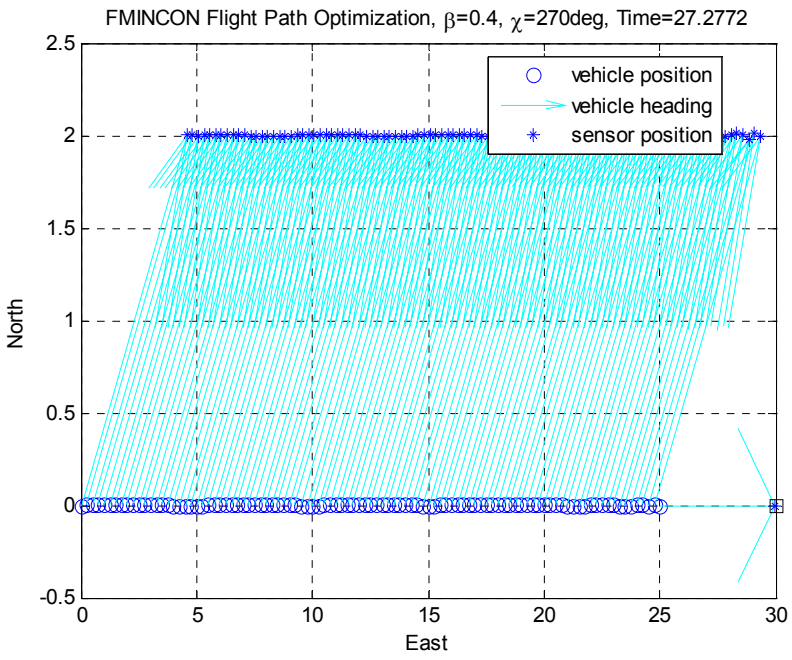

Figure 34 – Simulation for Analytical Solution

The flight path consists of a constant heading which offsets the wind. With this heading value known, Equations 63 through 65 are evaluated to determine the values of the Lagrange multipliers of the final co-states. These values are compared to those output form the simulation software and are shown below in Table 6.

Table 6 - Comparison of Analytical and Numerical Solution

	θ (deg)	υ^x	υ^y	υ^θ
Numerical Solution	23.5782	-1.0911	-0.4762	2.3813
Analytical Solution	23.5782	-1.0911	-0.4762	2.3810

This verifies the numerical solution found by the optimization software provides an optimal solution.

4.5 Urban Canyon Results

When attempting to fly through an urban canyon, the straight-line solution is utilized. The aircraft is instructed to fly the optimal path to the target, while minimizing the deviation from a line drawn directly between the starting point and the target. This path results in a set of initial minimum radius turns directing the aircraft at the target, followed by a straight line path, and is completed with the aircraft adjusting to put its sensor on the target at the required angle.

4.5.1 Flight Path Estimation

The original Dubins path that was created for the minimum time scenario could no longer be used for this method. Figure 35 below shows the modified Dubins flight path that was calculated as the initial guess for the optimization software.

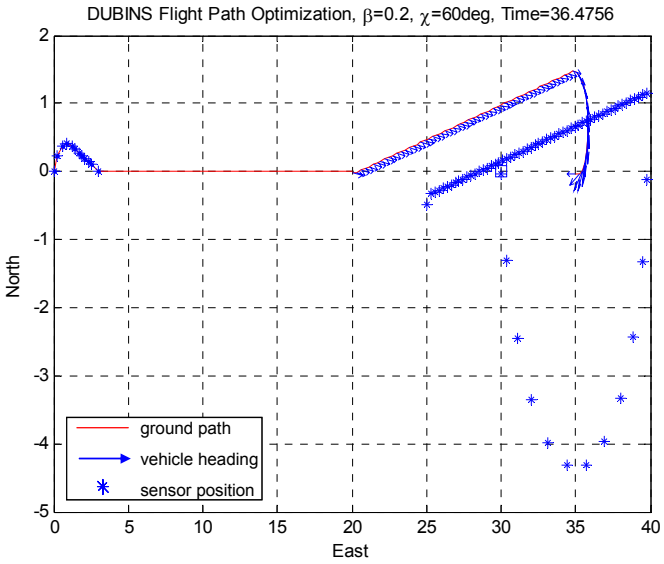

Figure 35 - Dubins Path Estimation for Urban Canyon Flight Path

Since the aircraft is instructed to fly the straight line path to the target, two Dubins paths were constructed. The first path estimates the aircraft's trajectory from the initial position and heading to the straight line solution. This path was accomplished in the length of three turn radiuses. Additionally, the sensor footprint was disregarded during this initial path since only the aircraft's position is of concern. The second Dubins path estimates the aircraft's trajectory starting at ten turn radii from the target while including the sensor footprint distance. The distances chosen for these results are not optimal; however, the estimated path is adequate for the optimization to obtain a solution.

4.5.2 Optimization Results

The results for the dynamic optimization are based off an initial set of parameters. These parameters, shown below in Table 7, were chosen as the base case for this scenario and will be referred to throughout this section. It should be noted that the initial heading angle has been changed from the minimum time scenario. For the urban canyon scenario, the vehicle is required to follow a desired path, and therefore the initial heading of the vehicle will be directed 45 degrees towards that path. Due to these requirements, the initial heading will not vary with the wind heading in this scenario.

Table 7 - Initial Parameters for the Urban Canyon Scenario

Start Position	(0,0)	Final Position	(30,0)
Initial heading	45^o	Final Heading	180^o
Wind Magnitude, β	0.2	Wind Direction, χ	60^o

Utilizing an estimated flight path from the Dubins path solution, the optimal flight path, per the base parameters, is determined and shown below in Figure 36.

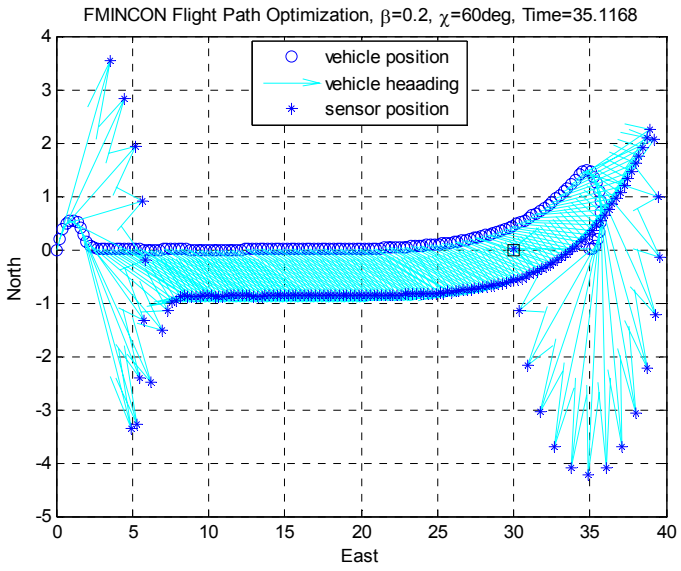

Figure 36 - Optimization Solution for Urban Canyon Scenario

This scenario was tested for robustness by varying three of the main parameters, wind heading, wind speed, and final target-viewing angle. These results are shown below and are displayed in the same manner as the minimum time scenario.

The first simulation varied the wind heading over 360 degrees in five-degree increments. Figure 37 below describes the surface plot for this simulation. The four sub-plots are described exactly as those for the minimum time scenario in Figure 17.

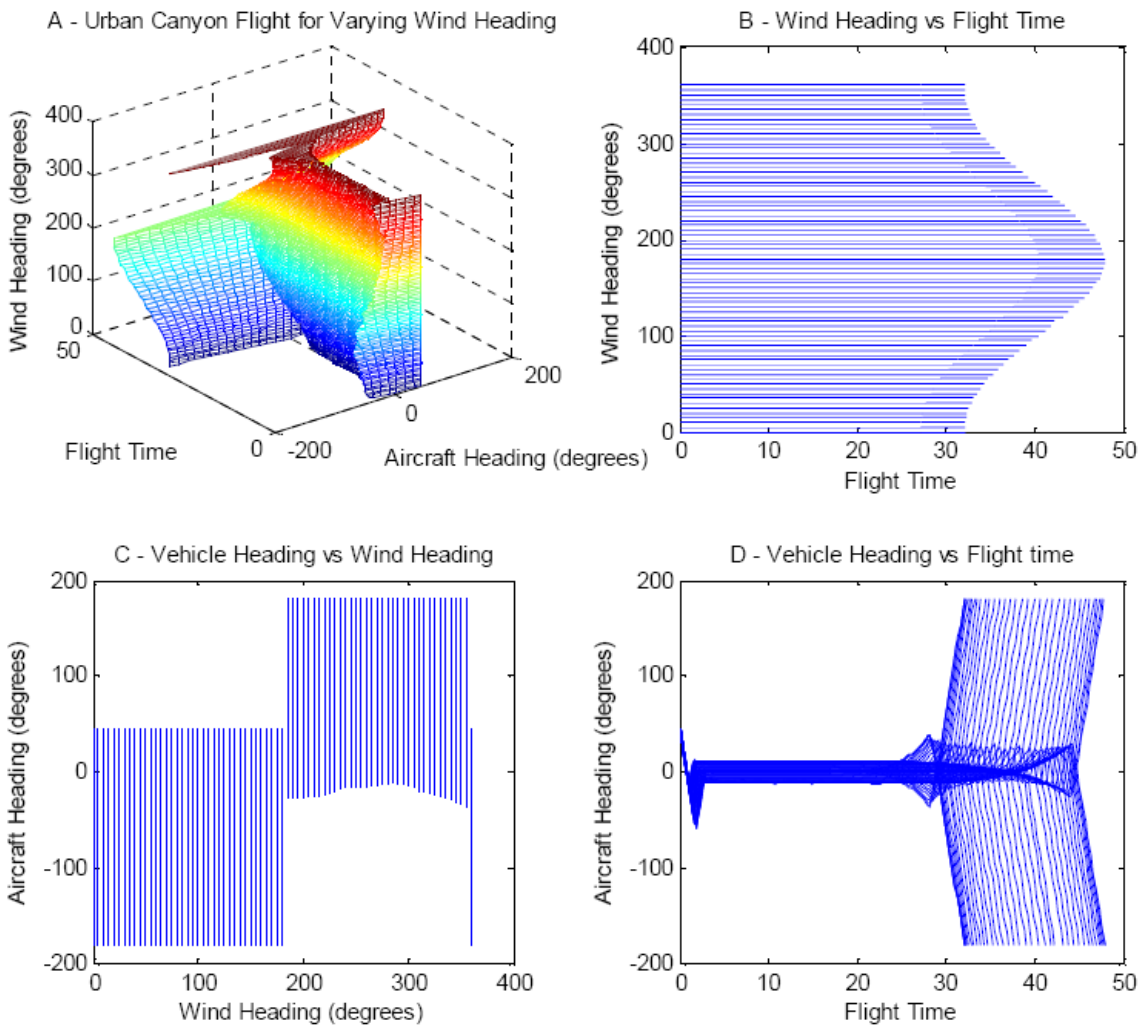

Figure 37 - Surface Plots - Varying Wind Heading with the Urban Canyon Scenario

These plots show consistent results over the course of the simulation. Figure 37B through D will be discussed further below for four individual wind headings. This will give a better indication of exactly what is occurring in these plots. The first plot to be evaluated compares the wind heading to the flight time and is shown below in Figure 38. This figure is a subset of Figure 37B, which shows accurate results as the flight time increases with an increasing head wind on the MAV.

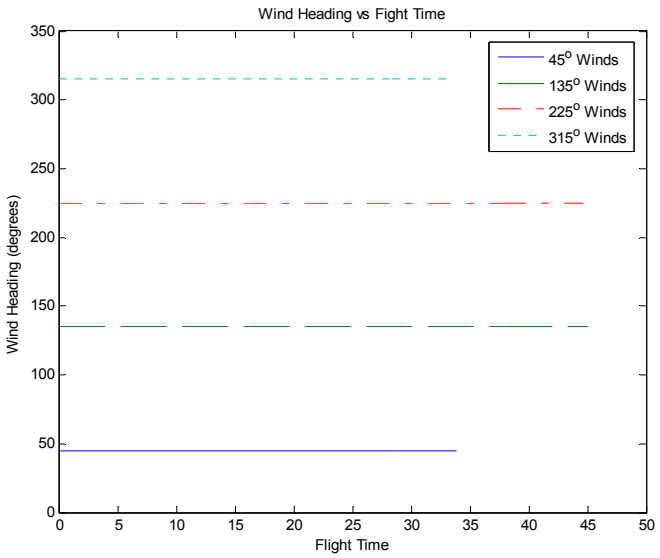

Figure 38 - Urban Canyon Wind Heading vs Flight Time; Varied Wind Heading

To get a better understanding of Figure 37C, Figure 39 below shows the vehicle's heading plotted against the wind heading. This plot describes the range of the vehicles heading over the course of an individual flight path. This range depends on the crab angle the aircraft must take to account for the direction of the wind and also indicates if the aircraft travels north or south of the target.

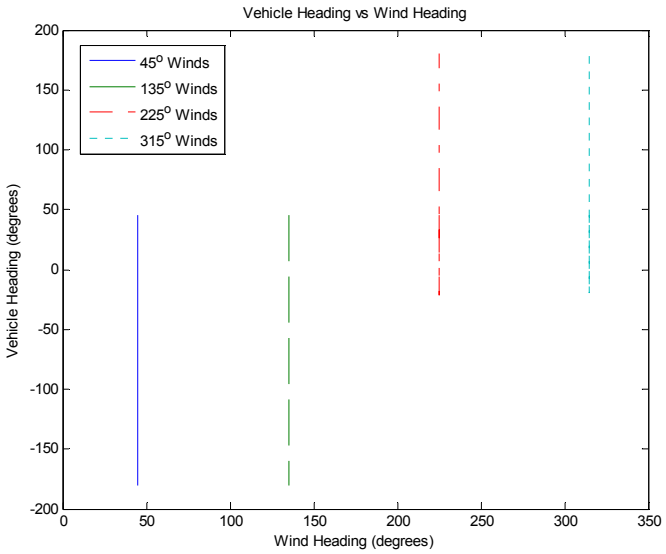

Figure 39 - Urban Canyon Aircraft Heading vs Wind Heading; Varied Wind Heading

Finally a subset of Figure 37D is described below in Figure 40. This figure shows the vehicle's heading over the course of the flight path. The initial curve in the figure describes the aircraft adjusting from an initial position to the straight line solution. The constant heading, shown in the center portion of the figure, accounts for the path cost which requires the MAV to fly directly to the target. The third portion of the figure describes the vehicle's headings for which the target will accurately be viewed.

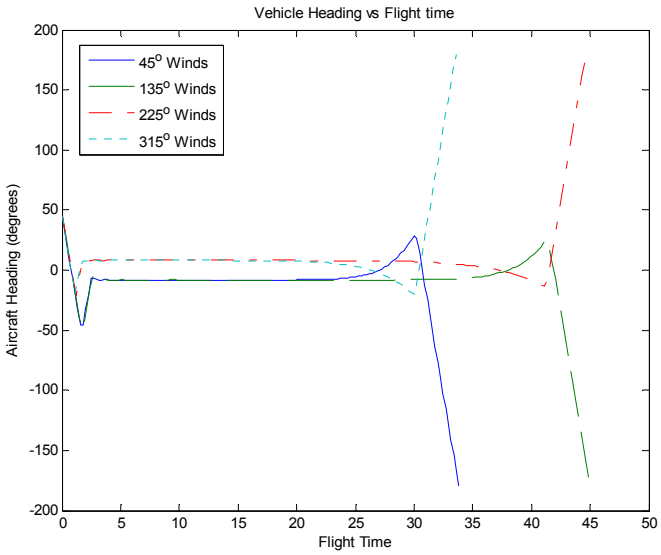

Figure 40 - Urban Canyon Vehicle Heading vs Flight Time; Varied Wind Heading

The second simulation run for this scenario varied the target viewing angle over 360 degrees in five degree increments. The parameters used for the simulation were the same as described in Table 7. Figure 41 below illustrates the surface plots developed from the simulation. The four sub-plots are described exactly as those for the minimum time scenario in Figure 21.

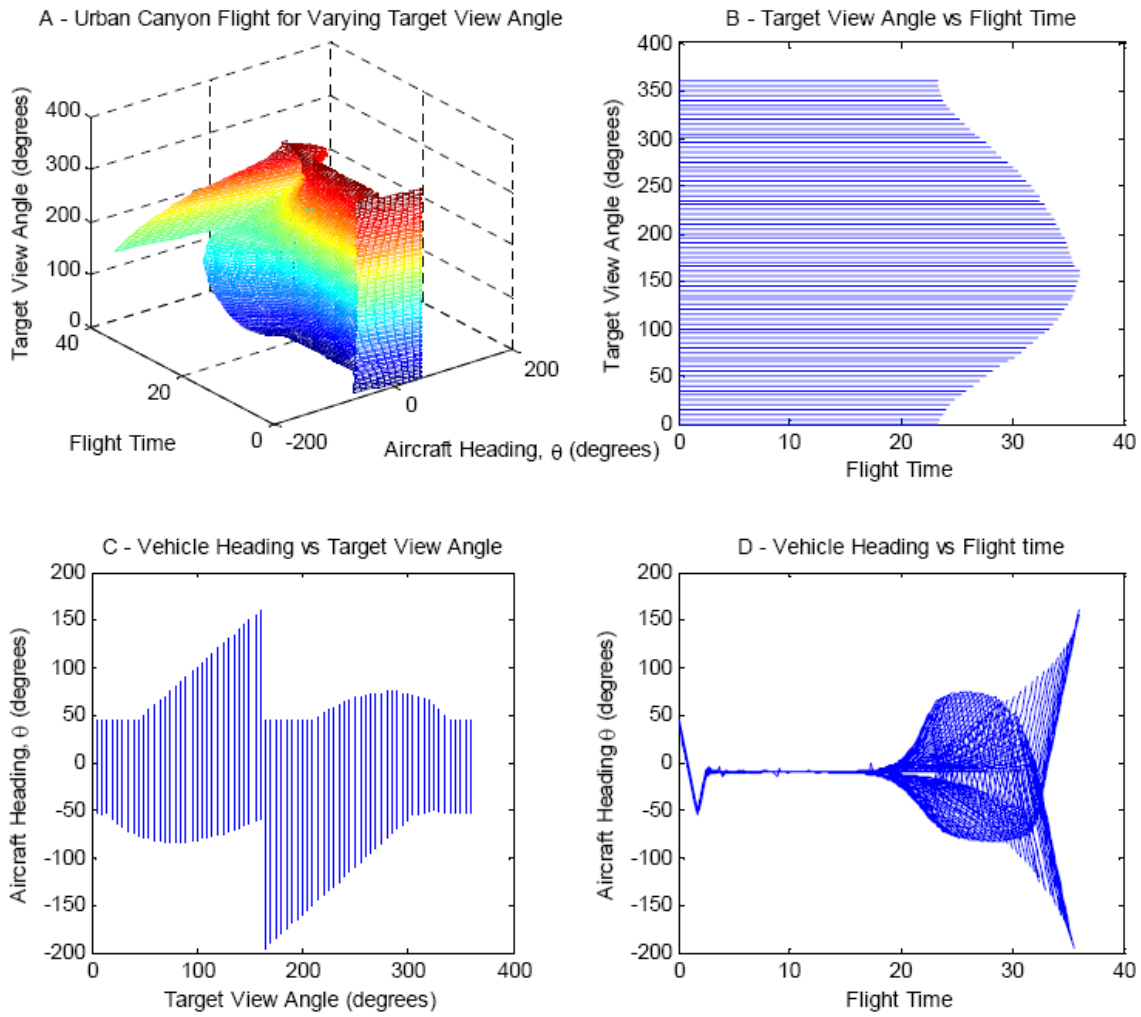

Figure 41 - Surface Plots - Varying Target Angle with the Urban Canyon Scenario

Figure 42 below describes a subset of Figure 41B. Four target viewing angles were chosen to better describe the plots in Figure 41. The results of this plot remain consistent with previous scenarios in that the flight time is heavily dependent on the angle at which the aircraft is required to view the target.

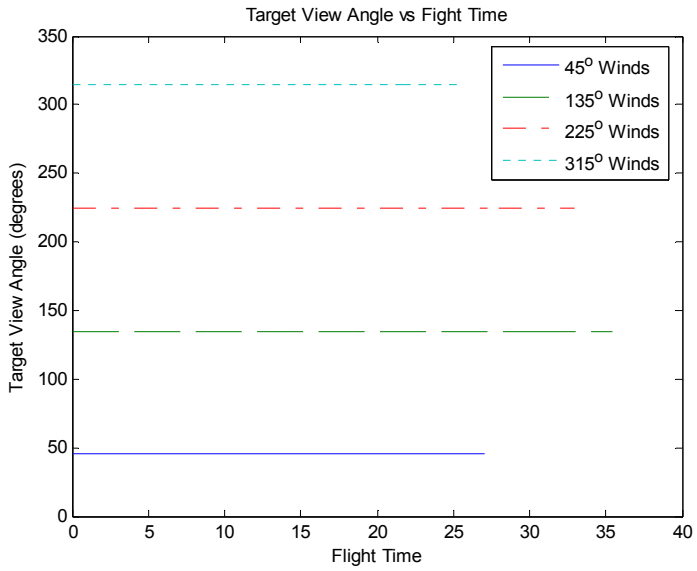

Figure 42 - Urban Canyon Wind Heading vs Flight Time; Varied Target Angle

Taking a closer look at Figure 41C, the vehicle's heading is plotted against the target viewing angle below in Figure 43. This describes the range in the aircraft's heading as the target viewing angle is varied. It can easily been seen that a greater heading range is needed when the target viewing angle is opposite the current aircraft heading.

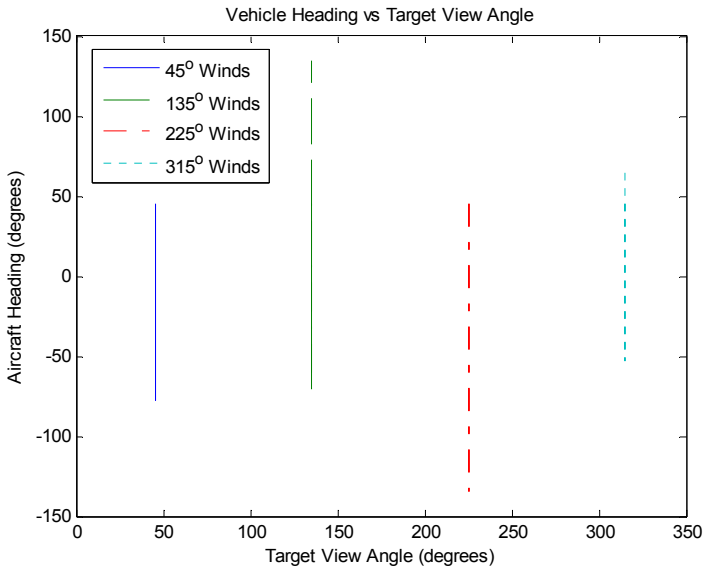

Figure 43 - Urban Canyon Aircraft Heading vs Wind Heading; Varied Target Angle

Finally, the vehicle's heading is plotted over the course of the flight and is shown below in Figure 44. This figure describes a subset of Figure 41D. The first curve, as well as the constant heading, remains unchanged throughout this simulation. The only variance in this plot is seen as the vehicle adjusts for the final target view angle.

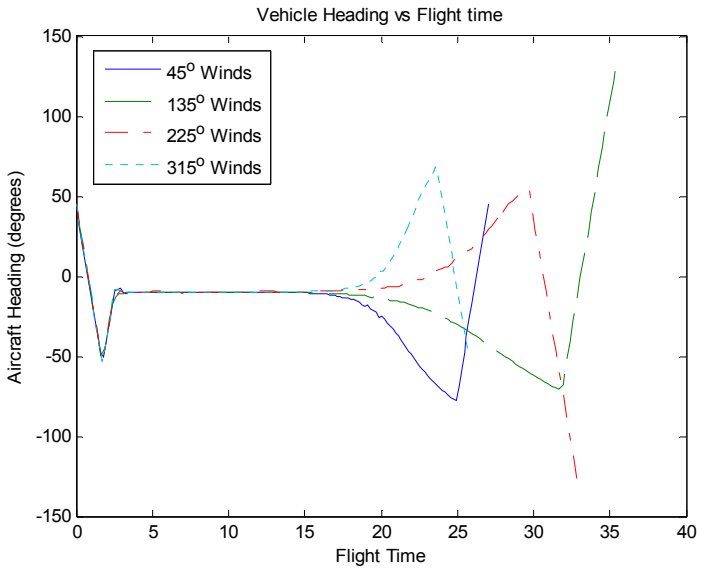

Figure 44 - Urban Canyon Vehicle Heading vs Flight Time; Varied Target Angle

The final simulation for this scenario varied the wind magnitude from zero to 70 percent of the aircraft's velocity. The surface plots for this case are shown below in Figure 45. The four sub-plots are described exactly as those for the minimum time scenario in Figure 25 and are described in more detail with four individual wind values.

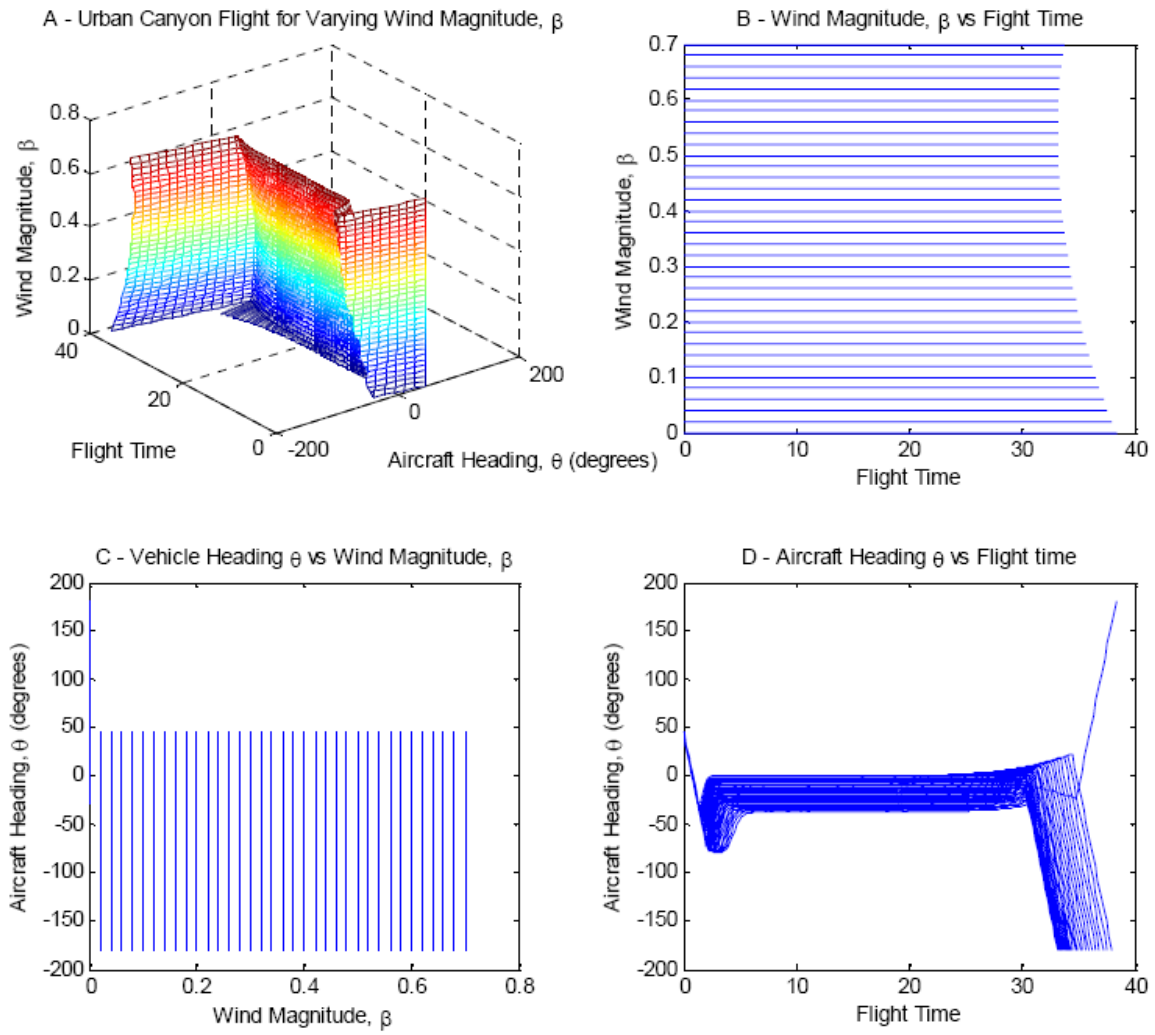

Figure 45 - Surface Plots - Varying Wind Magnitude with the Urban Canyon Scenario

Figure 45B is described in more detail below in Figure 46 for four individual flight paths. The results show that the minimum time flight under these parameters occurs at a wind speed of 54 percent of the MAV's velocity. This is better seen in Figure 45B and is a result of the MAV's crab angle taken to account for the wind. As the crab angle continues to increase to account for the wind, there comes a point where the vehicles velocity vector in the North direction will become greater then that of the East direction. This will result in a slower flight time. This transition occurs when $\beta = .54$.

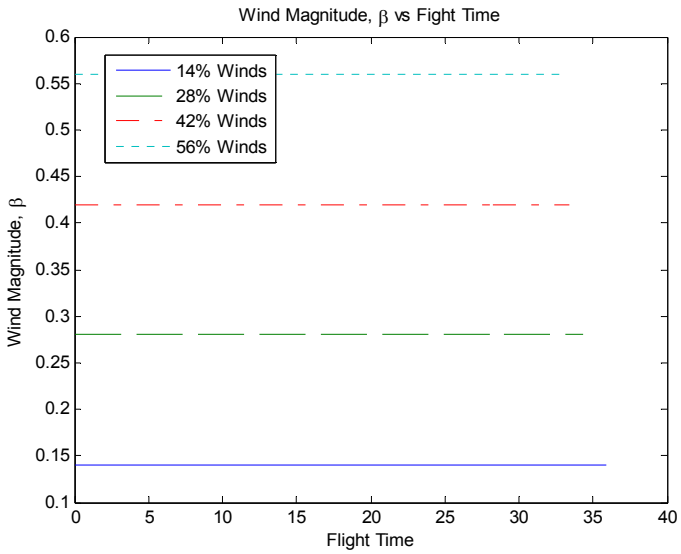

Figure 46 - Urban Canyon Wind Heading vs Flight Time; Varied Wind Magnitude

For this simulation, the ideal crab angle and the initial vehicle's heading differ by almost 90 degrees. Because of this, the range of the vehicle's headings throughout the flight profile is greatly varied and almost unchanged as the wind magnitude is increased. This is shown below in Figure 47, which describes a subset of Figure 45C.

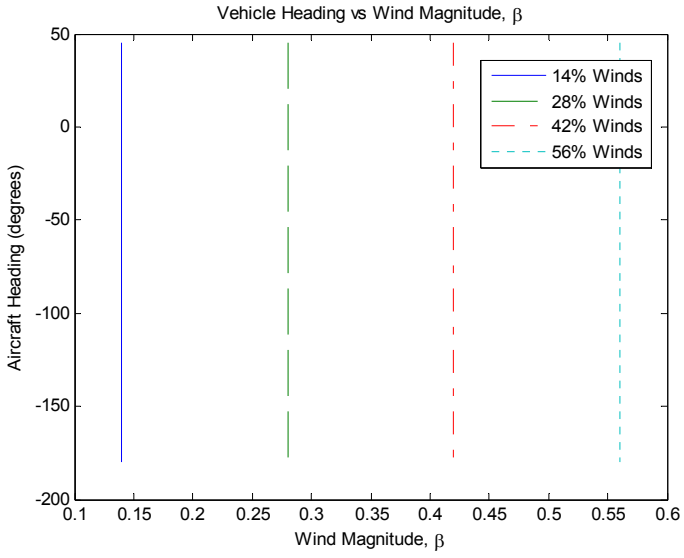

Figure 47 - Urban Canyon Aircraft Heading vs Wind Heading; Varied Wind Magnitude

Figure 48 below is a subset of Figure 45D and depicts the vehicle's heading over the course of the flight. This plot shows the same desired path being flown, however, the vehicle's heading is slightly offset as the winds continue to increase. This is representative of the vehicle's crab angle taken to account for the wind.

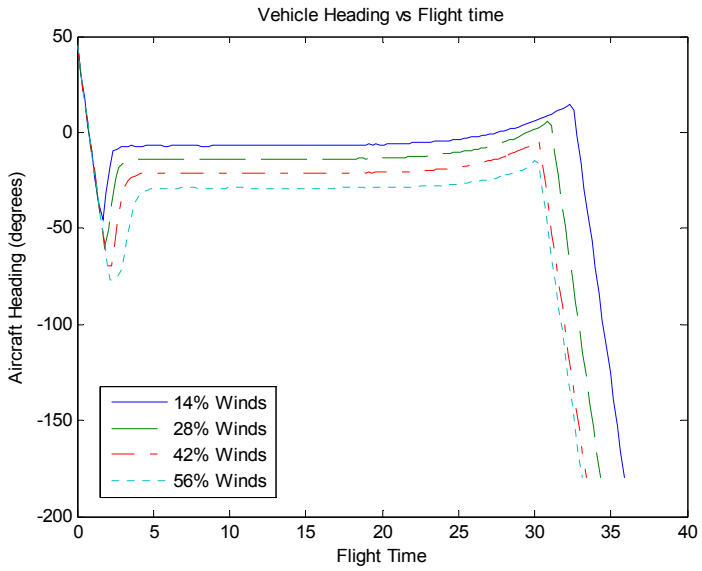

Figure 48 - Urban Canyon Vehicle Heading vs Flight Time; Varied Wind Magnitude

The three simulations run for this scenario prove the accuracy and robustness of the algorithm. With an initial heading constrained to approximately ± 45 degrees, an optimal path can be found for any wind heading and magnitude as well as any target viewing angle.

4.6 Target Tracking Results

In the previous scenarios, the aircraft has only been required to view the target at a desired angle. The follow scenario will consider the case where the aircraft must keep its sensor on the target for an extended period of time. In doing this, it will utilize both the

front and side sensor. The flight path will be a culmination of three optimal paths. The first will consist of a minimum time path to get the aircraft's forward sensor on the target. The second will be a transition stage, which consists of the aircraft adjusting its flight to put its side sensor on the target. The final stage is an orbital pattern for which the aircraft attempts to adjust for the wind, while continuously tracking the target with its side sensor.

4.6.1 Flight Path Estimation

For this case, the Dubins path will only be utilized for the initial flight path using the forward sensor. The final target angle given for the Dubins path is an angle of zero degrees. This will not be the most optimal path to get the sensor on target, but it is an adequate initial guess for the optimization to converge to an optimal solution. Figure 49 below shows the path estimation for the forward sensor.

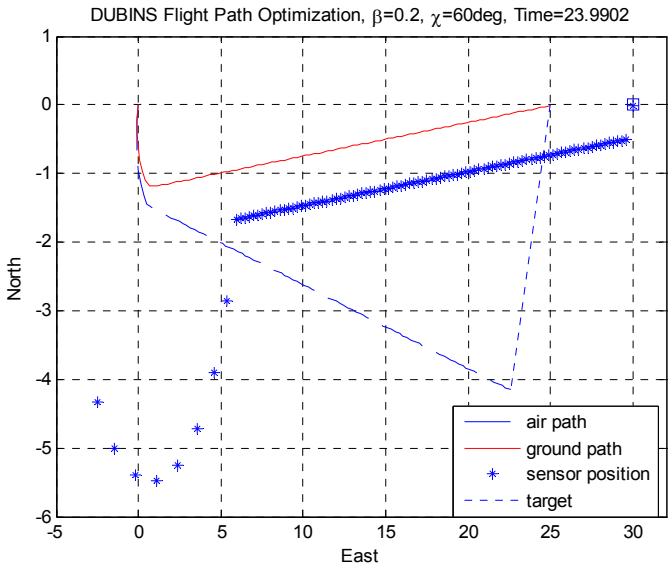

Figure 49 - Dubins Path for Dual Camera Scenario

For the next two path segments the initial guess for the flight path was hard coded into the software. Since the vertical angle of the side camera is fifteen degrees less than the forward sensor, it can be seen the aircraft will need to make a quarter turn in the direction opposite the sensor footprint prior to initiating its orbit. Therefore the flight path guess given to *fmincon* will consist of a maximum right turn. For the final orbital path, it was estimated that the aircraft should fly an orbit with a turn rate of approximately fifteen percent of the maximum. With this data given as the estimated flight path, *fmincon* was able to converge to a solution.

4.6.2 Optimization Results

The results for the dynamic optimization are based off an initial set of parameters. These parameters, shown below in Table 8, were chosen as the base case for this scenario and will be referred to throughout this section.

Table 8 - Initial Parameters for Dual Sensor Scenario

Start Position	(0,0)	Final Position	(30,0)
Initial heading	240^{o}	Final Heading	No constraint
Wind Magnitude, β	0.2	Wind Direction, χ	60^{o}

Below in Figure 50 the first stage of the flight path is shown. This is the optimum flight path the aircraft needs to fly in order to accurately put its forward mounted sensor on the target in the shortest period of time. A circle is also shown around the target which indicates the path the vehicle would take if there was no wind to alter the vehicles flight.

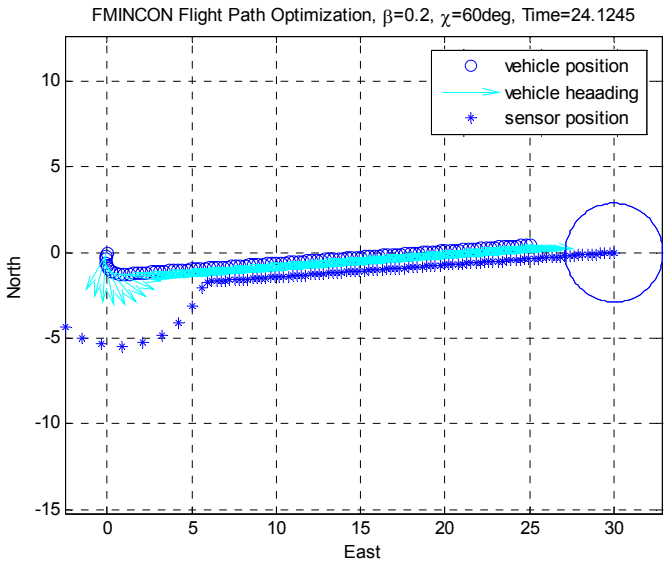

Figure 50 - Forward Sensor Dual Camera for Variable Winds

Figure 51 shows the second stage of the aircraft's flight as it transitions from the forward mounted sensor to the side mounted sensor. This depicts the minimum time solution to get the forward mounted sensor on the target followed by the side sensor.

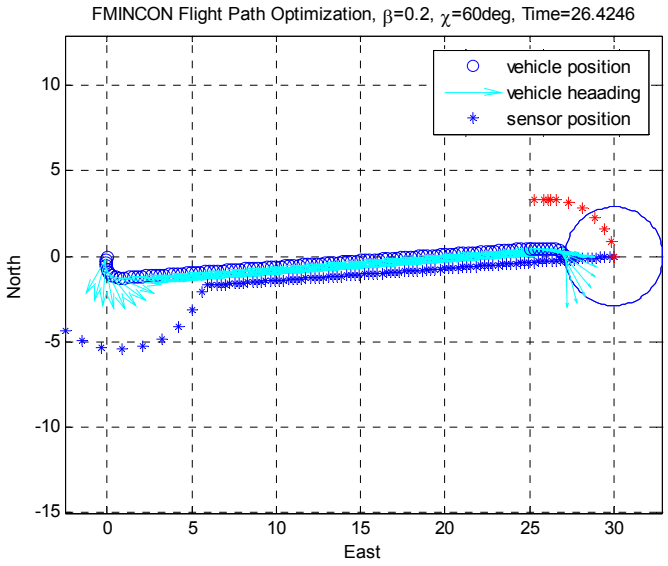

Figure 51 - Dual Sensor Transition for Variable Winds

Finally, Figure 52 shows the entire flight that will maximize the time the target can be viewed in a constant wind setting.

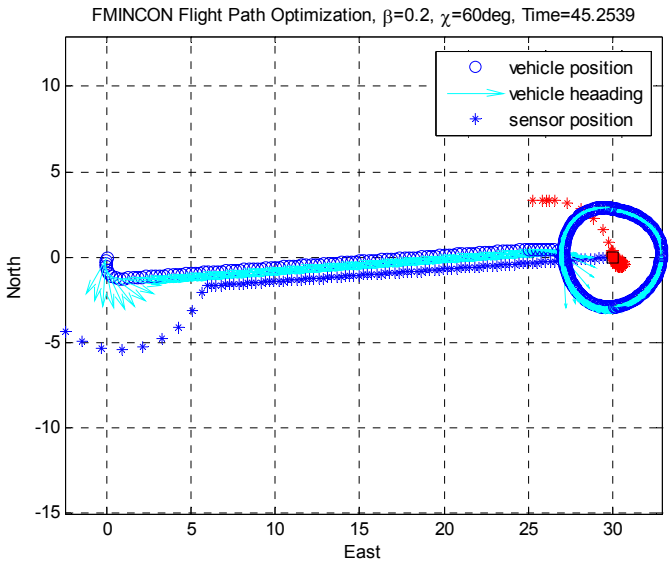

Figure 52 - Complete Dual Sensor Flight Path for Variable Winds

Assuming the wind magnitude was set to zero, the sensor footprint would remain on the target and the aircraft would fly a perfect circle around the target. However, when a constant wind is applied, it is impossible to continuously track the target with the vehicle modeled as point mass and a sensor footprint modeled as a point source. Therefore the flight path must be optimized to maximize the time the sensor is over the target.

To test the accuracy of the flight pattern, a circular sensor footprint was constructed. The radius of this footprint is varied to assure that the target is monitored at a minimum of 80 percent of the orbital flight path. For the flight path shown above in Figure 52, the target will be in view of the sensor footprint for 82% of the flight path with

a footprint radius of $0.64*r$, for r is equal to the distance of one turn radius. This radius will be calculated throughout this scenario to show the capabilities the sensor must obtain to accurately view a target over an orbital flight path.

In varying the wind heading and magnitude as well as the initial aircraft heading, the robustness of this scenario can be tested. Again, the initial heading will be based on the direction of the wind, for the aircraft will always take-off directly into the wind. Since the aircraft attempts to continually track the target at the end game, there is no need to vary the final target angle, as this will not alter the flight path. The results for these two cases are shown below.

The first test case varied the wind heading in five-degree increments over 360 degrees. The surface plot for this case is shown below in Figure 53. The four sub-plots are described exactly as those for the minimum time scenario in Figure 17.

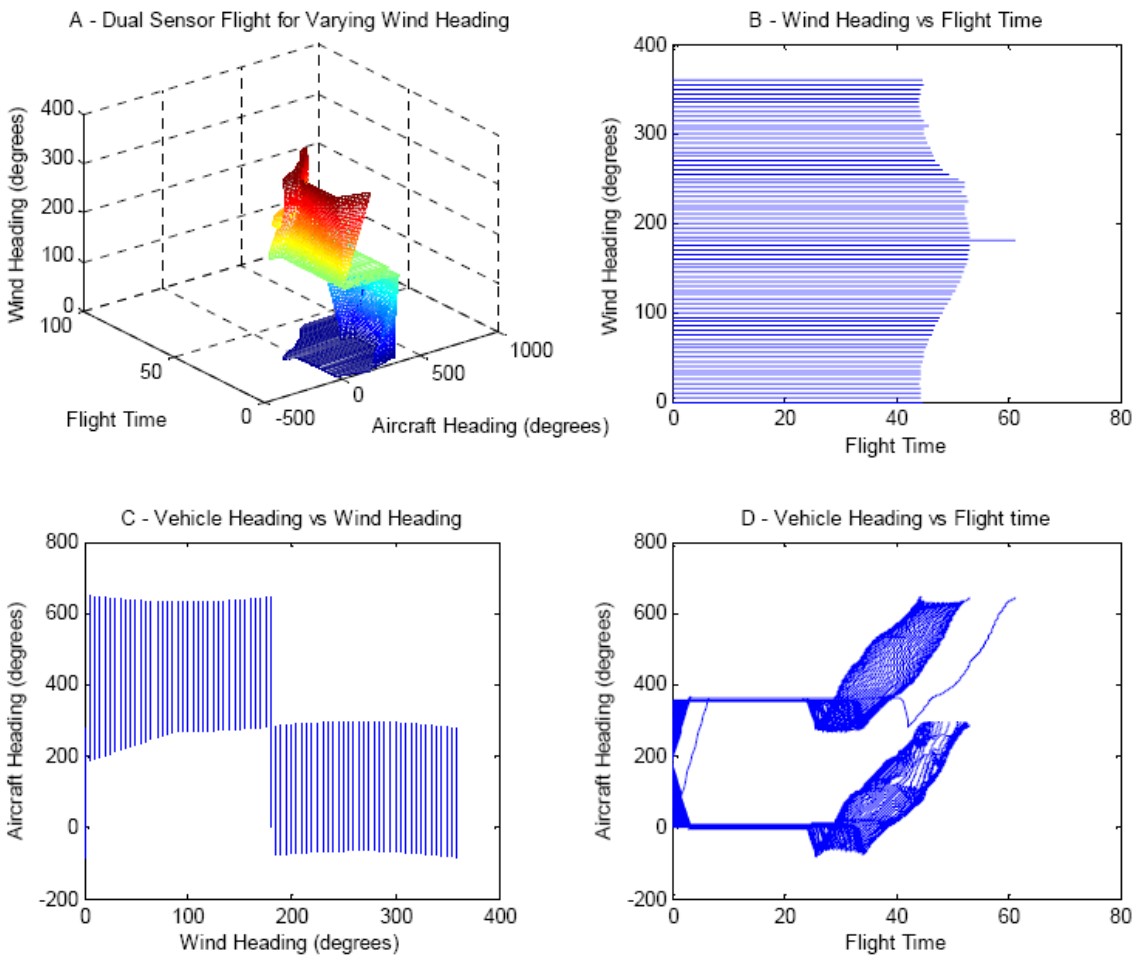

Figure 53 - Surface Plots - Varying Wind Heading with the Dual Sensor Scenerio

Although the surface plots are not completely smooth, it does show an accurate solution for the majority of the profiles tested. The angles that fail to remain consistent with the surface plot tend to increase their flight pattern on the orbital section perpendicular to the wind. This error is caused by the initial guess given to the simulation. This estimated flight path consists of a perfect circle, as if the wind magnitude was zero. This path estimation is not as accurate as it could be, and could be improved for future results.

Figure 54 below shows a closer look at Figure 53B and describes the total flight time as the wind heading is varied. These results remain consistent as the flight time increases with a greater head wind. It should be noted that the head wind only effects the vehicle in the first two stages of the flight. Once the aircraft starts the orbital path, there is little variance in the time of flight with regard to the wind heading.

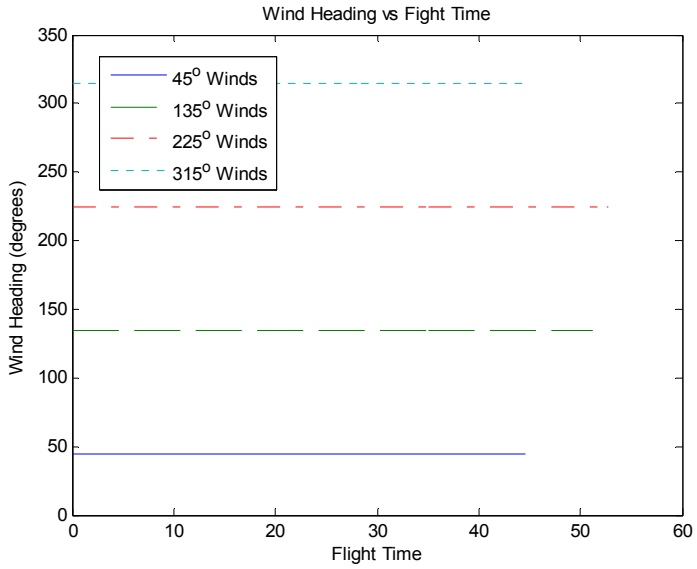

Figure 54 - Dual Sensor Wind Heading vs Flight Time; Varied Wind Heading

Taking a closer look at Figure 53C, Figure 55 below describes the range in aircraft heading as the wind heading is varied. However, since the vehicle flies the orbital pattern around the target, the aircraft's heading will range form 0 to 360 degrees as the results show below.

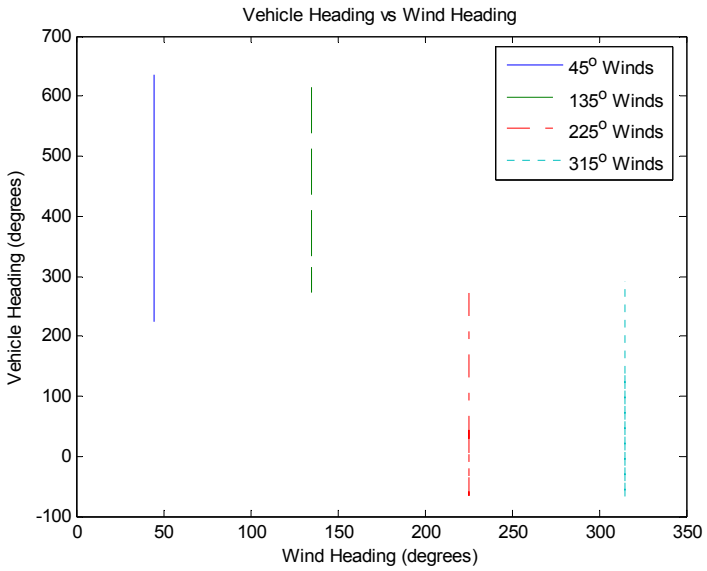

Figure 55- Dual Sensor Vehicle Heading vs Wind Heading; Varied Wind Heading

Figure 56 describes the aircraft's heading against the total flight time as the wind heading is varied. This plot is a subset of Figure 53D and shows the three different segments of the flight path. The first segment adjusts to the appropriate angle and flies straight until the forward sensor is on the target. The second segment depicts a decreasing heading value which describes the transition from the forward sensor to the side sensor. The final path shows the aircraft heading range of 360 degrees as the vehicle orbits the target.

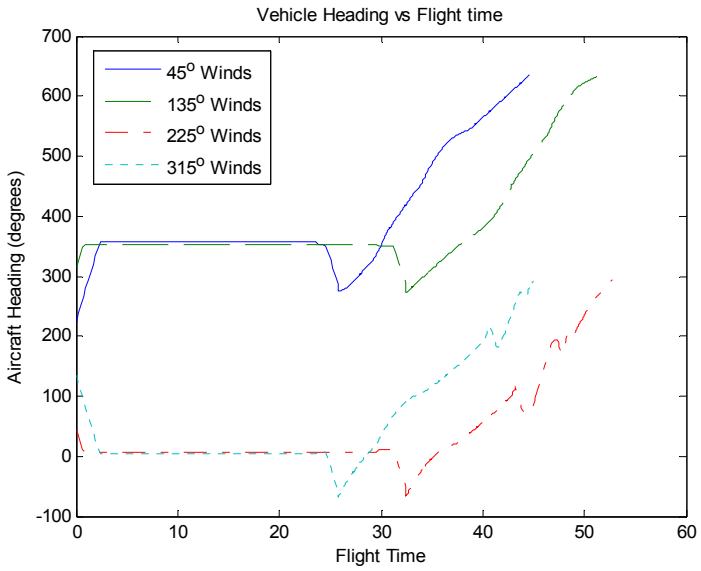

Figure 56 - Dual Sensor Vehicle Heading vs Flight Time; Varied Wind Heading

Finally, the sensor footprint is varied in size to assure the target is viewed for at least 80 percent of the flight. For the majority of the flight paths, the sensor footprint will remain under $0.8*r$. However, between the wind headings of 210 degrees and 240 degrees, the optimization reveals inconsistent results. This could be improved with a better initial estimation into the optimization software.

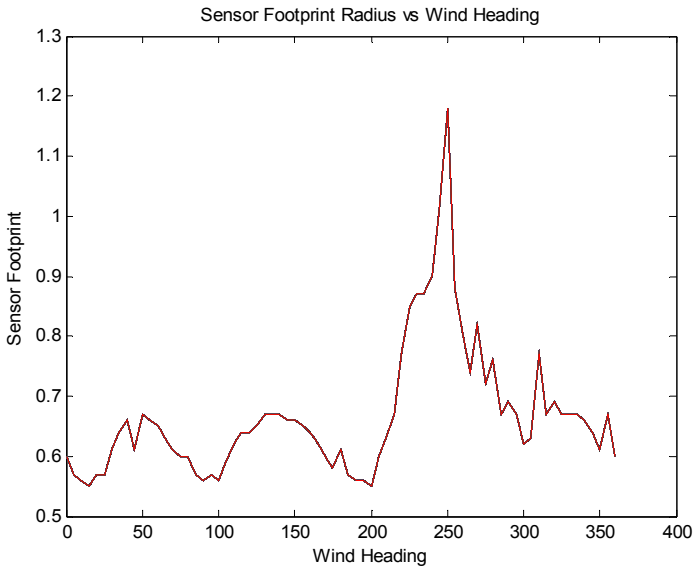

Figure 57 - Sensor Footprint Sensor for Varied Wind Heading

The second case tested for the target tracking scenario varied the wind magnitude from zero to 60 percent of the aircraft's velocity. The surface plots for this case are shown below in Figure 58. The four sub-plots are described exactly as those for the minimum time scenario in Figure 25.

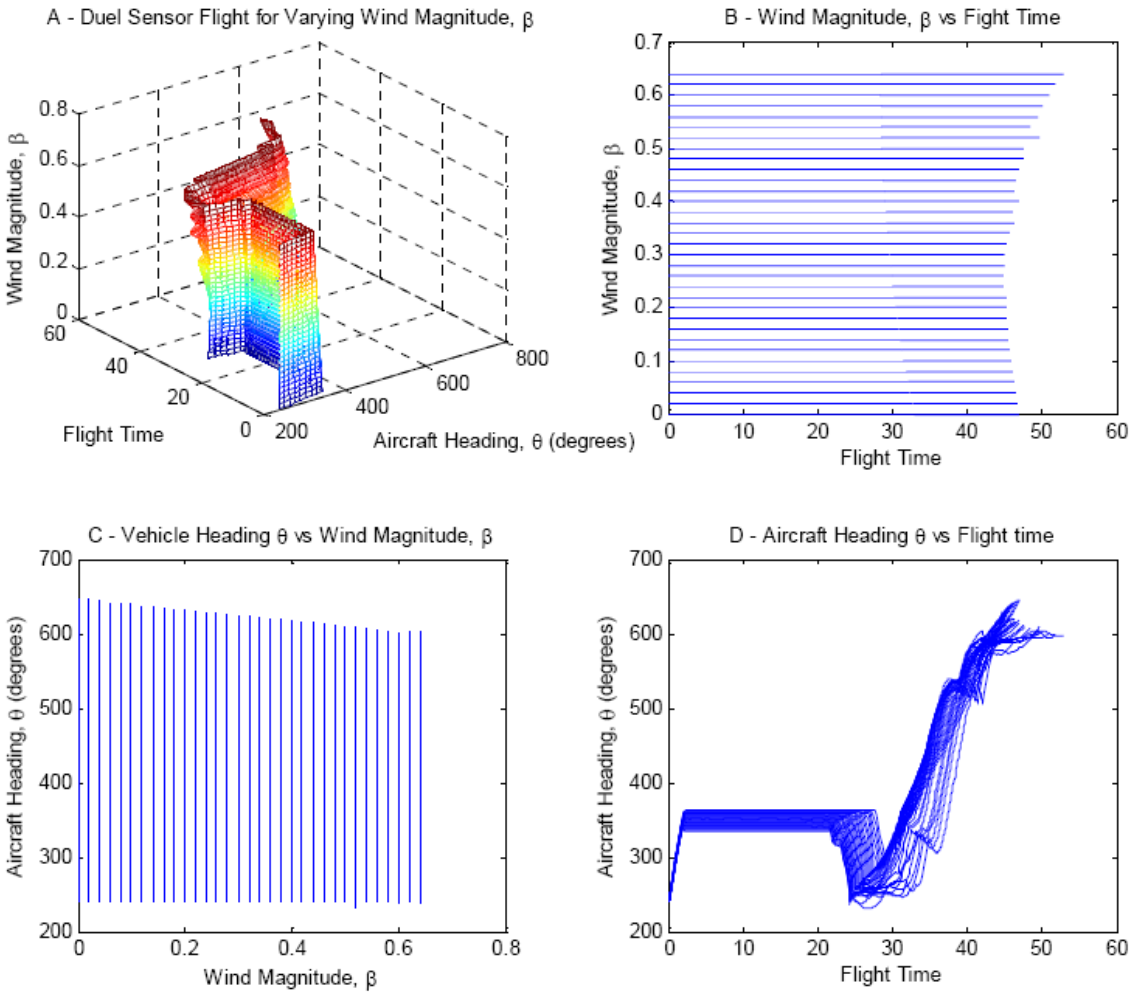

Figure 58 - Surface Plots - Varying Wind Magnitude with the Dual Sensor Scenerio

Figure 59 below describes the total flight time for a varying wind magnitude and is a subset of Figure 58B. Much like the results seen previously, the minimum flight time occurs when the combined velocity vectors of the wind and aircraft are greatest in the direction of the target. This takes place when $\beta = 0.24$.

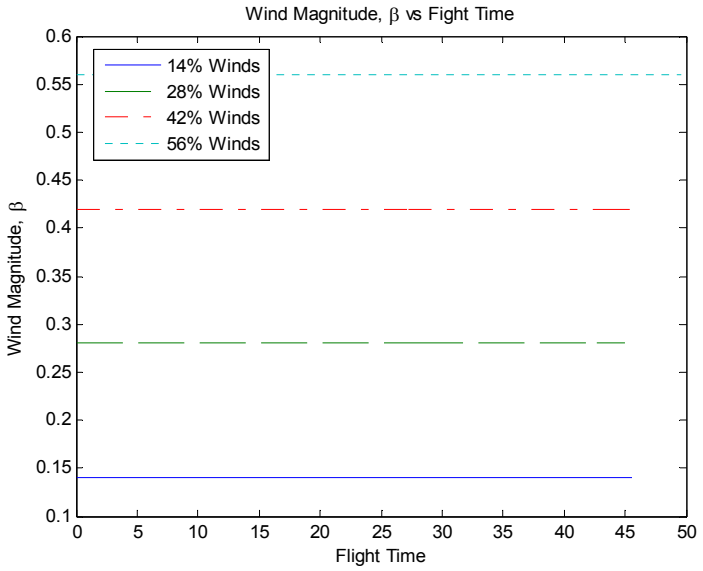

Figure 59 - Dual Sensor Wind Magnitude vs Flight Time; Varied Wind Magnitude

Again, with the orbital flight path, the aircraft's heading will range over 360 degrees as shown below in Figure 60. This is a subset of Figure 58C.

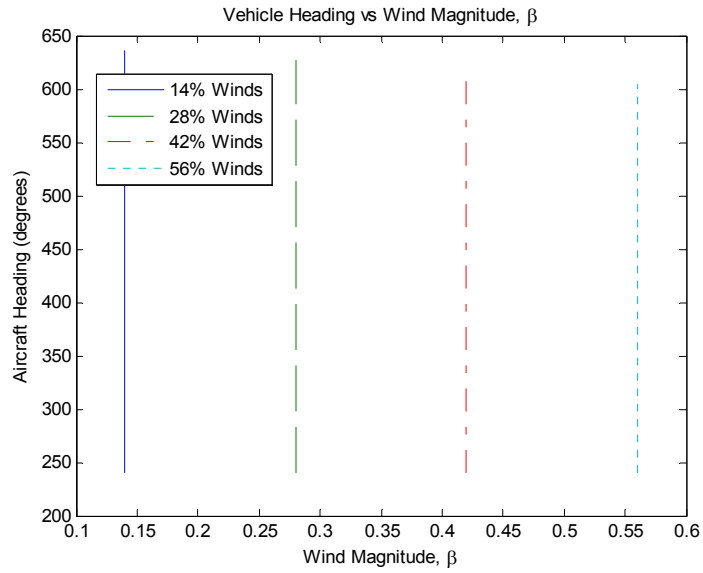

Figure 60 - Dual Sensor Vehicle Heading vs Wind Magnitude; Varied Wind Magnitude

Figure 61 below describes the aircraft's heading plotted against the total flight time as the wind magnitude is increased. This is a subplot of Figure 58D above and shows the

increasing difficulty the simulation has in providing smooth results in the orbital flight pattern as the winds are increased.

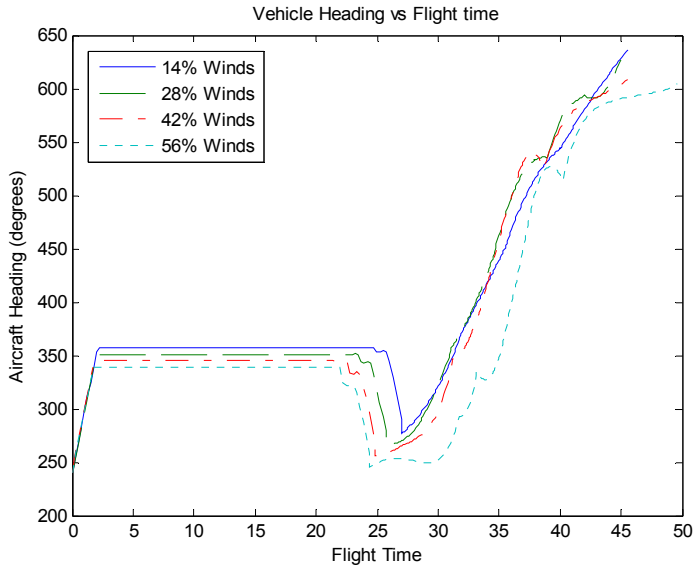

Figure 61 - Dual Sensor Vehicle Heading vs Flight Time; Varied Wind Magnitude

Finally the sensor footprint radius is plotted as the wind magnitude is increased. In order to assure the target is in view of the sensor footprint at least 80 percent of the time, the size of the footprint will continue to increase as the wind magnitude increases. This is shown below in Figure 62 and proves to be accurate due to the immense crab angle the aircraft will be forced to take as the strength of the wind continues to grow in magnitude.

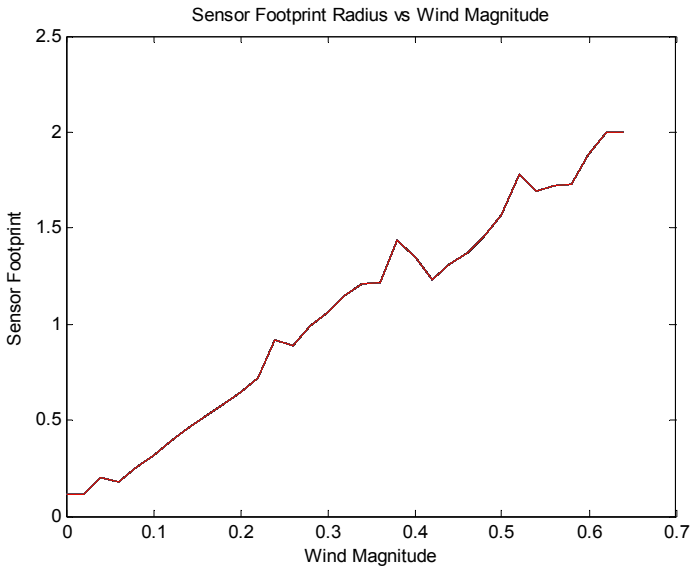

Figure 62 - Sensor Footprint Radius for Varied Wind Magnitude

4.7 Chapter Summary

The results presented in this chapter cover the three flight path scenarios. Each scenario has been tested for robustness and repeatability. Overall, the optimizations were successful, and optimal flight paths have been calculated for a wide range of data. Additionally, an analytical solution was evaluated for the minimum time scenario. Although a closed-form solution for the control could not be determined, evaluation of the co-states did verify the results of the optimization. Finally, the Dubins path results used as the initial guess for the dynamic optimization proved to be the most valuable and important step in determining an optimal solution. Without an accurate initial guess, the optimization run time is increased by an order of magnitude and many times, a solution could not be found.

5. Conclusions and Recommendations

5.1 Conclusions

This research accomplished all of the objectives described in Chapter 1.

- Initially, L.E. Dubins theories were exploited to develop a flight path which was effectively used as an initial guess for the dynamic optimization problem. A Dubins path was utilized in two different methodologies. The first path considered flight from an initial position and heading to a final position and heading. This flight path was used for both the minimum time scenario as well as the dual sensor scenario. The second path was comprised of two Dubins path runs. The first run considered flight from an initial point and heading to a straight line heading directed at the target in a relatively short distance. The second run then considered the flight path at the end game, which developed a path from a straight line heading directed at the target to the final viewing angle. Each of these paths provided adequate information to the optimization software for an optimal solution to be found given the scenarios presented in this research.
- With a valid estimation of the flight path, the minimum time scenario was solved. Optimization techniques were utilized to determine an optimal flight path starting at an initial position and heading and ending with a desired viewing angle of the target. This scenario was tested with varying wind headings and magnitude, initial headings, and final viewing angles. The solution technique developed, which used Dubins path as an initial guess for the dynamic optimization problem,

proved to be very robust given the conditions presented in this research, and converged very quickly.

- The next objective considered a MAVs flight through an urban canyon. This scenario restricted the flight path in width, as if the vehicle was forced to fly between two buildings before viewing the target. The solution for this scenario utilized a minimum time terminal cost as well as path cost that forced the vehicle to minimize the difference between its flight angle and the straight line angle between the starting position and the target. Although adequate results were obtained for this scenario, it was not as robust as the solutions obtained in the minimum time case. The struggle to obtain fully robust results validates the necessity for providing a valid initial guess to the optimization. Even though the initial guess provided by the Dubins path was a decent solution for the majority of the cases, it could be improved to better cover the range of variables tested.
- The final objected exploited both the forward sensor and a side sensor mounted on the vehicle to view the target for any continuous duration of time. Again, the initial guess provided to the system proved to be a factor in acquiring robust results. However, adequate solution were obtained over the range of each variable.

These results lay out a benchmark that can be used in future work to compare the robustness and effectiveness of a control law designed for MAVs operating in wind. Future work will consist of implementing variable wind into the optimization simulation.

Once those results are acquired, additional research will consider developing a control law that will give real time updates of variable wind to the flight control autopilot to autonomously correct the aircraft's flight path to an optimum trajectory. Ideally, this solution will compare very closely to the simulation results displayed in this research.

5.2 Recommendations

With any academic research, there is a time constraint for which results must be published. Given more time for this research, the following outlines improvements that could be made to better utilize the optimization software. These improvements would result in a larger range of solutions to the flight path optimization problem.

- Throughout this research, it has been shown that an adequate estimation of the desired flight path is essential in solving for the optimal solution. For the minimum flight time scenario, Dubins path provided a very good estimation of the optimal path. This allowed the optimization software to iterate on that estimation to find an optimal solution. However, it was seen in the urban canyon scenario as well as the dual sensor scenario that optimization results were heavily affected by a path estimation that was not as good as it could have been. Although the results from this research were still effective, providing a better flight path estimation could result in a complete solution to any desired flight path. Therefore, utilizing L.E. Dubins theories to better predict these flight sceneries, including flight patterns in close proximities, would drastically improve the robustness of these optimizations.

- The results of this research are based on a first-order Euler discretization of the equations of motion. In an attempt to increase the fidelity of the model, it would be beneficial to use a different method for discretization. By increasing the order of the discretization, both the optimization results and the analytical solution may be improved. The new model would give the optimization software more information when iterating for an optimal flight path, and that additional information could provide beneficial when determining the analytical solution.
- In evaluating the dual sensor scenario, the aircraft model is described as a point mass with the control to the equations of motion only consisting of the turn rate, ω. This requires the aircraft to remain wings level as it flies an orbital pattern around the target. In practice, this would require a combination of rudder and aileron control to achieve the desired path. By incorporating an aircrafts bank angle into the model, a more realistic solution can be obtained. Wind effects could be better accounted for using the additional control, and the aircraft's orientation would be more consistent with a typical flight profile.
-

Finally, additional research will lead to the development of a control law for closed-loop operations with a flight autopilot. The implementation of this control law will lead to a vehicle's test flight. Once this has occurred, the flight path chosen by the autopilot can be compared to the optimal paths acquired from this research to determine the effectiveness of the controller.

APPENDIX A: MATLAB CODE DIAGRAMS

1. Matlab code diagram and definitions for the minimum time forward sensor flight path.

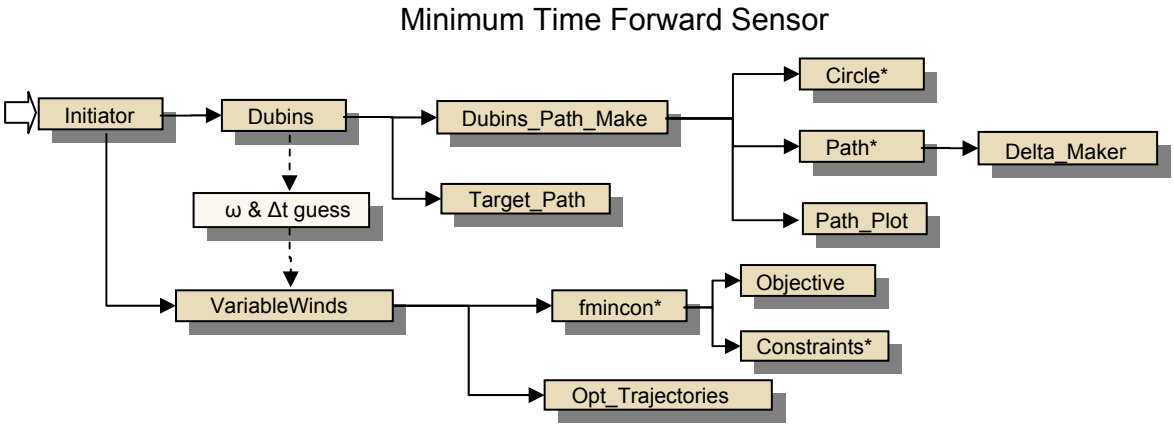

- **Initiator** - This function defines all the parameters for the optimization. These parameters are then fed into both the Dubins function as well as the VariableWinds function.
- **Dubins** - This function is called by initiator and runs the required functions to develop the Dubins Path. Dubins iterates on the solutions to solve for the rendezvous point of the virtual target and the a/c. Additionally, the turn rate and time step developed in this path are fed to the VariableWinds function as the optimal flight path estimation.
- **Dubin_path_maker** - This function is called by Dubins and is the core of the Dubins code. This m file creates both the air and ground paths for the vehicles flight.
- **Target_path** - This function is called by Dubins and determines the path of the virtual target effected by the constant wind.
- **Dubin_circle** - This function is called by Dubins and creates the four circles used in the dubins path method.

- **Path** – This function is called by dubins_path_maker to develop the four flight paths resulting from Dubins methodology.
- **Path_Plot** – This function is called by dubins_path_maker and plots the shortest of the four Dubins paths.
- **Delta_maker** - This function is called by dubins_path_maker and determines the increment size (step size) of the Dubins path. It adjoins the paths of the first curve, straight portion, and final curve of the path and makes the step size equal for the complete path.
- **VariableWinds** - This function is called by initiator and runs all the dynamic optimization. The objective function, constraint function, and optimality function are contained in this m-file.
- **Fmincon –** This function is called by VariableWinds and utilizes both the objective function as well as the constraint function to determine the optimal control for the system.
- **Opt_Trajectories –** This function is called by VariableWinds and utilized the optimal control found by the fmincon function to determine a solution for the states.
- **Objective –** This function is called by fmincon and describes the objective function, or Cost J, which is the desired function to be minimized.
- **Constraints –** This function is called by fmincon and describes the constraints places on the states of the system.

2. Matlab code diagram and definitions for the minimum time side sensor flight path. Those functions not defined below are identical to those of the time forward sensor flight path.

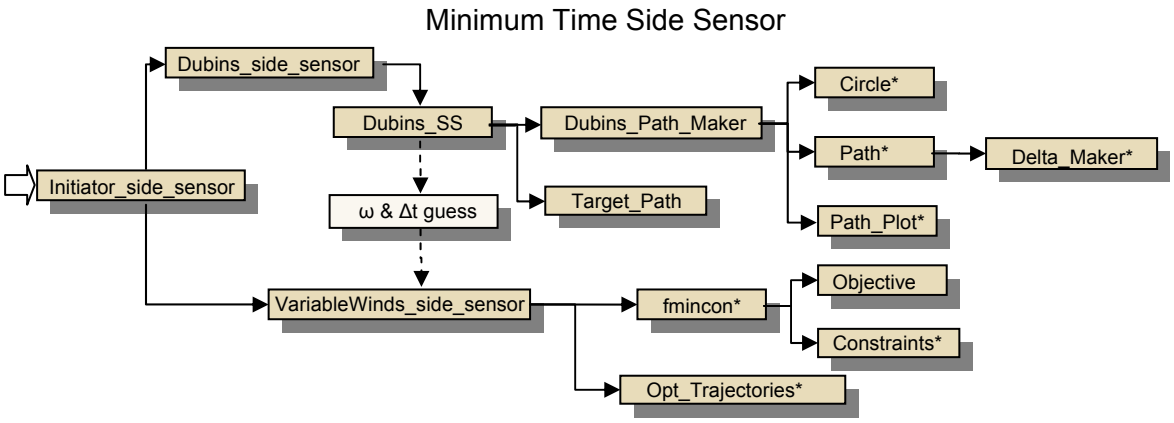

- **Initiator_side_sensor** - This function defines all the parameters for the optimization. These parameters are then fed into both the Dubins_side_sensor function as well as the VariableWinds function.
- **Dubins_side_sensor** - This function is called by initiator_side_sensor and iterates for the shortest dubins path over multiple positions on a circle encompassing the target.
- **Dubin_SS** - This function is called by Dubins_side_sensor and solves for the shortest path based on the parameters given without regard to sensor footprint position.
- **VariableWinds_side_sensor** - This function is called by initiator_side_sensor and runs the dynamic optimization for a vehicle with a side mounted sensor. The objective function, constraint function, and optimality function are contained in this m-file.

3. Matlab code diagram and definitions for the Urban Canyon Flight Path. Those functions not defined below are identical to those of the time forward sensor flight path.

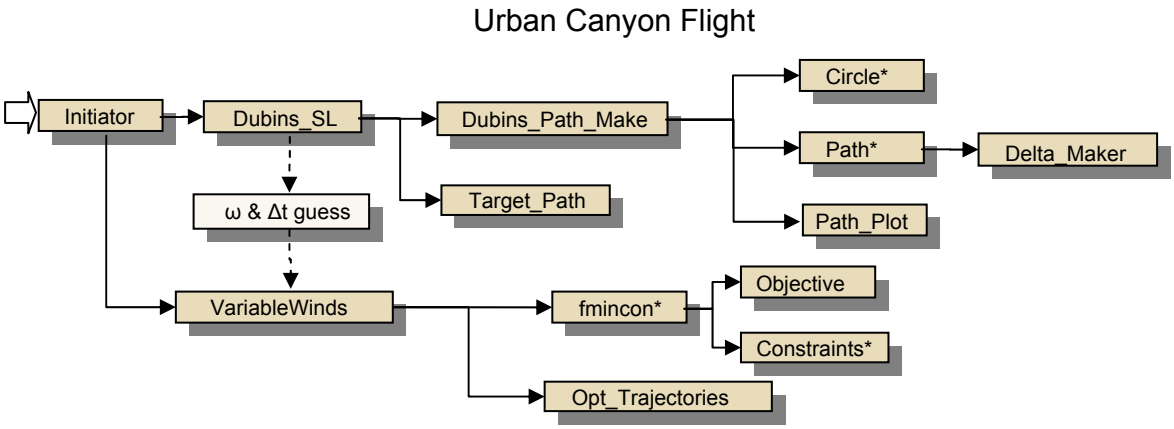

- **Dubin_SL** - This function is called by initiator and determins two separate Dubins paths. Each path is combined to form one path and this path is used as the estimated flight path to the dynamic optimization.

4. Matlab code diagram and definitions for the Dual Sensor Flight Path. Those functions not defined below are identical to those of the time forward sensor flight path.

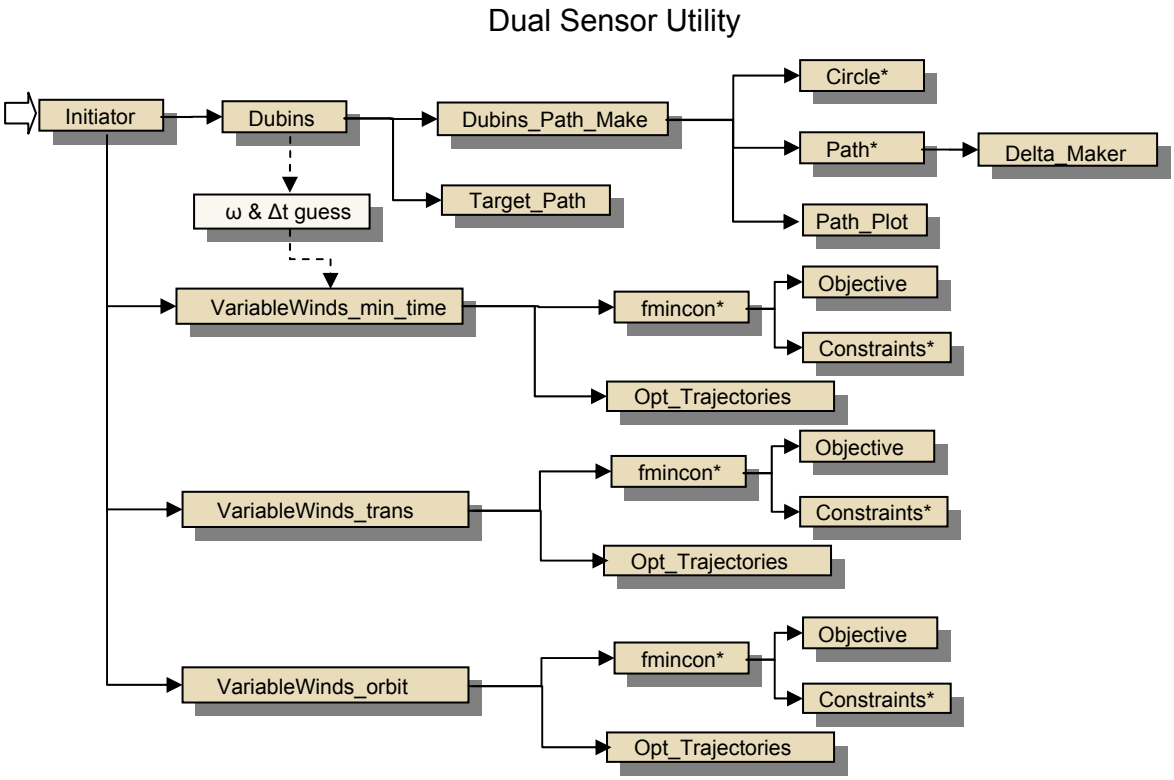

- **VariableWinds_min_time** - This function is called by initiator and runs the dynamic optimization for the minimum time portion of the flight.. The objective function, constraint function, and optimality function are for the minimum time portion are contained in this m-file.
- **VariableWinds_trans** - This function is called by initiator and runs the dynamic optimization for the transition flight from the forward sensor on the target to the side sensor on the target. The objective function, constraint function, and optimality function for the side sensor are contained in this m-file.

- **VariableWinds_orbit** - This function is called by initiator and runs the dynamic optimization for the orbital flight path utilizing the side sensor. The objective function, constraint function, and optimality function for the orbital solution are contained in this m-file.

Bibliography

Bryson, A., *Dynamic Optimization.* Addison-Wesley; Menlo Park, CA. 1999.

Bryson, A., *Applied Optimal Control (Revised Printing).* Hemisphere Publishing Co. 1975.

Bui, X., Boissonnat, J., Soueres, P. and Laumond, J. "Shortest Pth Synthesis for Dubins Non-holonomic Robot." *IEEE International Conference on Robotics and Automation,* Vol.1. May 1994.

Dubins, L., "On Curves of Minimal Length with a Constraint on Average Curvature, and with Prescribed Initial and Terminal Positions and Tangents." *American Journal of Mathematics,* Vol. 79, No. 3 (Jul., 1957), pp. 497-516.

Gordon, R. *Optimal Dynamic Soaring for Full Size Sailplanes.* MS Thesis. AFIT/GAE/ENY06-S04. Department of Aeronautics and Astronautics, Air Force Institute of Technology, OH. September 2006.

Higgs, T. *Modeling, Stability, and Control of a Rotatable Tail on a Micro-Air Vehicle.* MS Thesis. AFIT/GAE/ENY/06-D05. Department of Aeronautics and Astronautics, Air Force Institute of Technology, OH. December 2005.

Hull, D., "Conversion of Optimal Control Problems into Parameter Optimization Problems." *Journal of Guidance, Control, and Dynamics,* Vol. 20, No. 1, January-February 1997.

Jacques, D., "Functional Optimization and Optimal Control" Air Force Institute of Technology, OH. 2002.

Larson, R., Mears, M. and Blue, P., "Path Planning for Unmanned Air Vehicles to Goal States in Operational Environments." *AIAA,* 2005.

Larson, R.., Pachter, M. and Mears, M. "Path Planning by Unmanned Air Vehicle for Engaging an Integrated Radar Network." *AIAA Guidance, Navigation, and Control Conference and Exhibit*, CA, August 2005.

McGee, T., Spry, S. and Hedrick, K., "Optimal Path Planning in a Constant Wind with a Bounded Turning Rate." *AIAA Guidance, Navigation, and Control Conference and Exhibit*, CA, August 2005.

Miller, G., Jacques, D. and Pachter, M., "Trimmed Flight Control." *AIAA Guidance, Navigation, and Control Conference and Exhibit,* TX, August 2003.

Office of the Secretary of Defense. *Unmanned Aerial Vehicles Roadmap 2005 – 2030.* Washington: HQ DOD, August 2005.

Osborne, J., Rysdyk, R. "Waypoint Guidance for Small UAVs in Wind." University of Washington, WA. September 2005.

Pachter, M., *Optimal Trajectories for Cooperative Classifications.* Kluwer Academic Publishers; Netherlands. 2003.

Rafi, F., Khan, S., Shafiq, K. and Shah, M., "Autonomous Target Following by Unmanned Aerial Vehicles." Department of Computer Science. University of Central Florida, FL. 2006.

Robinson, B. *An Investigation into Robust Wind Corrected Algorithms for Off-the-Shelf Unmanned Aerial Vehicle Autopilots.* MS Thesis. AFIT/GAE/ENY/06-J14. Department of Aeronautics and Astronautics, Air Force Institute of Technology, OH. June 2006.

Rysdyk, R., "UAV Path Following for Target Observation in Wind." University of Washington, WA. 2006.

Vaughn, A. *Path Planning and Control of Unmanned Aerial Vehicles in the Presence of Wind.* MS Thesis. Department of Mechanical Engineering, University of California at Berkeley, CA. Fall 2003.

Vita

First Lieutenant Michael D. Zollars graduated from Beavercreek High School in Beavercreek, Ohio. He entered undergraduate studies at the Pennsylvania State University in State College, Pennsylvania where he graduated with a Bachelor of Science degree in Mechanical Engineering in May 2003. He was commissioned through Detachment 720 AFROTC at the Pennsylvania State University where he received a Regular Commission.

After completing training, he was assigned to the 746 Test Squadron, Holloman AFB, New Mexico. While there, he performed duties as a flight test engineer evaluating navigation technologies onboard the C-12J aircraft, and led research efforts within the navigation field. In August 2005, he entered the Graduate School of Engineering and Management, at the Air Force Institute of Technology. Upon graduation, he will be assigned to Air Force Research Labs, Air Vehicles Directorate at Wright-Patterson AFB, Ohio.

REPORT DOCUMENTATION PAGE	Form Approved OMB No. 074-0188

The public reporting burden for this collection of information is estimated to average 1 hour per response, including the time for reviewing instructions, searching existing data sources, gathering and maintaining the data needed, and completing and reviewing the collection of information. Send comments regarding this burden estimate or any other aspect of the collection of information, including suggestions for reducing this burden to Department of Defense, Washington Headquarters Services, Directorate for Information Operations and Reports (0704-0188), 1215 Jefferson Davis Highway, Suite 1204, Arlington, VA 22202-4302. Respondents should be aware that notwithstanding any other provision of law, no person shall be subject to an penalty for failing to comply with a collection of information if it does not display a currently valid OMB control number.
PLEASE DO NOT RETURN YOUR FORM TO THE ABOVE ADDRESS.

1. REPORT DATE *(DD-MM-YYYY)*	**2. REPORT TYPE**	**3. DATES COVERED** *(From – To)*
03-22-2007	**Master's Thesis**	Sep 2005 – Mar 2007

4. TITLE AND SUBTITLE

OPTIMAL WIND CORRECTED FLIGHT PATH PLANNING FOR AUTONOMOUS MICRO AIR VEHICLES

5a. CONTRACT NUMBER

5b. GRANT NUMBER

5c. PROGRAM ELEMENT NUMBER

6. AUTHOR(S)

Zollars, Michael, D., 1st Lieutenant, USAF

5d. PROJECT NUMBER

5e. TASK NUMBER

5f. WORK UNIT NUMBER

7. PERFORMING ORGANIZATION NAMES(S) AND ADDRESS(S)
Air Force Institute of Technology
Graduate School of Engineering and Management (AFIT/EN)
2950 Hobson Way
WPAFB OH 45433-7765

8. PERFORMING ORGANIZATION REPORT NUMBER

AFIT/GAE/ENY/07-M28

9. SPONSORING/MONITORING AGENCY NAME(S) AND ADDRESS(ES)
AFRL/VAC
2130 Eighth St, WPAFB, OH 45433
Dr. Jeffrey Tromp
937.255.3900
AFIT Proposal #2003-120, AFIT JON #05-186

10. SPONSOR/MONITOR'S ACRONYM(S)

11. SPONSOR/MONITOR'S REPORT NUMBER(S)

12. DISTRIBUTION/AVAILABILITY STATEMENT
APPROVED FOR PUBLIC RELEASE; DISTRIBUTION UNLIMITED.

13. SUPPLEMENTARY NOTES

14. ABSTRACT

This research effort focuses on determining the optimal flight path required to put a micro air vehicle's (MAVs) fixed sensor on a target in the presence of a constant wind. Autonomous flight is quickly becoming the future of air power and over the past several years, the size and weight of autonomous vehicles has decreased dramatically. As these vehicles were implemented into the field, it was quickly discovered that their flight paths are severely altered by wind. However, since the size of the vehicle does not allow for a gimbaled camera, only a slight perturbation to the attitude of the vehicle will cause the sensor footprint to be displaced dramatically. Therefore, the goal of this research was to use dynamic optimization techniques to determine the optimal flight path to place a MAV's sensor footprint on a target when operating in wind for three different scenarios. The first scenario considered the minimum time path given an initial position and heading and a final position and heading. The second scenario minimized the error between the MAV's ground track and a straight line to the target in order to force a desired path on the vehicle. The final scenario utilized both a forward mounted sensor as well as a side mounted sensor to optimize the time the target is continually in view of the sensor footprint. Each of these scenarios has been captured in simulated plots that depict varying wind angles, wind speeds, and initial and final heading angles. These optimal flight paths provide a benchmark that will validate the quality of future closed-loop wind compensation control systems.

15. SUBJECT TERMS
Autonomous Navigation, UAV, MAV, Wind, Wind Corrected, Target Recognition, Optimization

16. SECURITY CLASSIFICATION OF:			**17. LIMITATION OF ABSTRACT**	**18. NUMBER OF PAGES**	**19a. NAME OF RESPONSIBLE PERSON**
REPORT	**ABSTRACT**	**c. THIS PAGE**			Paul A. Blue, Maj, USAF (ENY)
U	**U**	**U**	**UU**	118	**19b. TELEPHONE NUMBER** *(Include area code)* (937) 255-3636, ext 4714; e-mail: Paul.Blue@afit.edu

Standard Form 298 (Rev: 8-98)
Prescribed by ANSI Std. Z39-18